UNIVERSIDADE FEDERAL DO RIO GRANDE DO SUL
INSTITUTO DE MATEMÁTICA E ESTATÍSTICA
PROGRAMA DE PÓS-GRADUAÇÃO EM MATEMÁTICA APLICADA

Modeling and Simulation of Pollutant Generation in the Combustion of Biodiesel Surrogates

por

Silvia Barcelos Machado

Tese submetida como requisito parcial
para a obtenção do título de

Doutora em Matemática Aplicada

Prof. Dr. Álvaro Luiz de Bortoli
Orientador

Porto Alegre, fevereiro de 2022.

CIP - CATALOGAÇÃO NA PUBLICAÇÃO

Barcelos Machado, Silvia

Modeling and Simulation of Pollutant Generation in the Combustion of Biodiesel Surrogates / Silvia Barcelos Machado.—Porto Alegre: PPGMAp da UFRGS, 2022.

99 p.: il.

Tese (doutorado)— Universidade Federal do Rio Grande do Sul, Programa de Pós-Graduação em Matemática Aplicada, Porto Alegre, 2022.
Orientador: Luiz de Bortoli, Álvaro

Tese: Matemática Aplicada: Dinâmica de Fluidos,
CFD, Methyl Decanoate, NO_x, Soot

Modeling and Simulation of Pollutant Generation in the Combustion of Biodiesel Surrogates

por

Silvia Barcelos Machado

Tese submetida ao Programa de Pós-Graduação em Matemática Aplicada do Instituto de Matemática e Estatística da Universidade Federal do Rio Grande do Sul, como requisito parcial para a obtenção do título de

Doutora em Matemática Aplicada

Linha de Pesquisa: Dinâmica de Fluidos

Orientador: Prof. Dr. Álvaro Luiz de Bortoli

Banca examinadora:

Prof. Dr. Antônio J. da Silva Neto
IPRJ/UERJ

Prof. Dr. Leandro Farina
PPGMAp/UFRGS

Prof. Dr. Nilson R. Marcílio
PPGEQ/UFRGS

Prof. Dr. Régis S. de Quadros
PPGMMAT/UFPEL

Tese defendida em
Fevereiro de 2022.

Prof. Dr. Lucas da Silva Oliveira
Coordenador

CONTENTS

LIST OF FIGURES . . . . . **vii**

LIST OF TABLES . . . . . **x**

LIST OF ABBREVIATIONS AND SYMBOLS . . . . . **xi**

ABSTRACT . . . . . **xv**

RESUMO **1**

1 INTRODUCTION **2**

1.1 Motivation 2

1.2 General Objectives 3

1.3 Specific Objectives 3

1.4 Structure of the thesis 4

2 BIOFUELS AND POLLUTANTS **5**

2.1 Biodiesel 7

2.1.1 Methyl Decanoate 11

2.2 Pollutants 12

2.2.1 NO_x 13

2.2.2 Soot 15

3 KINETIC MECHANISMS **17**

3.1 Mechanism Reduction Techniques 18

3.1.1 Directed Relation Graph 19

3.2 Kinetic Mechanisms for MD 21

3.3 Kinetic Mechanisms for NO_x 24

3.3.1 Thermal Mechanism 24

3.3.2 Fenimore Mechanism 26

3.3.3 N_2O-intermediate Mechanism 26

3.3.4 NNH Mechanism 27

3.4 Kinetic Mechanisms for Soot 28

3.4.1 C_2H_2-intermediate Model 28

3.4.2 Semi-empirical Model 29

4 METHODOLOGY 33

4.1 Mixture Fraction 33

4.1.1 Burke-Schumann Solution 36

4.1.2 Mixture Fraction with Multi-parameters 43

4.2 Reactive Flow Equations 44

4.3 Turbulent Flow 47

4.3.1 Turbulent Viscosity 51

4.4 Dimensionless Equations 52

5 PROBLEM SETUP 55

5.1 Turbulent Jet Diffusion Flame 55

5.2 Computational Domain and Mesh 58

5.3 Initial Conditions and Boundary Conditions 58

6 NUMERICAL SOLVERS 63

6.1 Finite Difference Method 63

6.2 Rosenbrock Method 64

7 NUMERICAL RESULTS 67

7.1 Results for NO_x 72

7.2 Results for Soot 80

8 FINAL CONCLUSIONS 85

BIBLIOGRAPHY 99

LIST OF FIGURES

2.1 Global transesterification process. 8

2.2 Biodiesel FAME and biodiesel surrogates [89]. 11

3.1 Direct Relation Graph Sketch. 20

5.1 Diffusion flame sketch. 56

5.2 Free jet sketch. 57

5.3 Burner sketch. 58

5.4 Two-dimensional mesh sketch in the x and y-directions. 59

7.1 Mixture fraction field of MD flame in the range [0,8]. 67

7.2 Comparison of the numerically obtained mixture fraction with experimental data [8] in the centerline of the MD flame. 68

7.3 Comparison with experimental data [64] for: (a) O_2 mass fraction and (b) H_2O mass fraction, as a function of the mixture fraction (Z), in a methanol flame. 69

7.4 Comparison with experimental data [64] for: (a) CO_2 mass fraction and (b) temperature (K), as a function of the mixture fraction (Z), in a methanol flame. 70

7.5 Comparison of numerical results with experimental data [39] for: (a) NO molar fraction obtained by the Zel'dovich mechanism; (b) NO molar fraction obtained using Zel'dovich and N_2O-intermediate mechanisms, along the mixture fraction (Z) in a methanol flame. 71

7.6 Comparison with experimental data [64] for: (a) O_2 mass fraction and (b) CO and CO_2 mass fraction, as a function of the mixture fraction (Z), in a MD flame. 72

7.7 Comparison with experimental data [64] for the temperature, as a function of the mixture fraction (Z), in the MD flame. 73

7.8 Comparison of numerical results with experimental data [39] for: (a) NO molar fraction obtained by the Zel'dovich mechanism; (b) NO molar fraction obtained using the Zel'dovich and N_2O-intermediate mechanisms, along the mixture fraction (Z) in a MD flame. 74

7.9 Comparison with experimental data [84] for: (a) CO_2 mass fraction and (b) H_2O mass fraction in a MD flame. 75

7.10 Comparison with experimental data [84] for: (a) CH_4 mass fraction and (b) OH mass fraction in a MD flame. 76

7.11 Comparison with experimental data [84] for: (a) C_2H_2 mass fraction and (b) C_2H_4 mass fraction in a MD flame. 77

7.12 Temperature (K) field of MD flame. 77

7.13 Comparison with experimental data [84] for temperature (K) in a MD flame. 78

7.14 Comparative temperature (K) error [84] in a MD flame. 78

7.15 Molar fraction of NO obtained by: (a) Zel'dovich mechanism; (b) Zel'dovich and N_2O-intermediate mechanisms, in a MD flame. 79

7.16 NO mass fraction field. 79

7.17 Comparison with experimental data [47] for: (a) C_2H_2 mass fraction and (b) OH mass fraction in a MD flame. 81

7.18 Comparison with experimental data [47] for: (*a*) Y_{C_S} mass fraction and (*b*) N_S particle number density in a MD flame. 81

7.19 Comparison with experimental data [21] for: (*a*) C_2H_2 mass fraction and (*b*) C_2H_3 mass fraction in a MD flame. 82

7.20 Comparison with experimental data [21] for soot volume fraction in a MD flame. 83

7.21 Soot mass fraction in a MD flame. 84

7.22 Soot mass fraction field. 84

LIST OF TABLES

2.1 Annual World Ethanol Production (million gallons). 6

2.2 Biodiesel production in 2020 (billion liters). 7

2.3 Chemical formulation of the main fatty acids in biodiesel. 9

2.4 Nomenclature of the chemical species represented by NO_x. 14

3.1 Simplified Mechanism for MD. Units are mol, cm^3, s, K and cal/mol. 23

3.2 Kinetic parameters of the extended Zel'dovich mechanism. Units are mol, cm^3, s, K and cal/mol. 25

3.3 Kinetic parameters of the N_2O-intermediate mechanism. Units are mol, cm^3, s, K and cal/mol. 27

3.4 Kinetic parameters of the soot formation mechanism by [47]. Units are mol, cm^3, s, K and cal/mol. 29

5.1 Parameter conversion. 60

6.1 Parameters for the fourth-order Rosenbrock method. 66

7.1 Maximum values of CO and CO_2 mass fractions. 73

7.2 Maximum values of the NO mass fractions. 74

LIST OF ABBREVIATIONS AND SYMBOLS

List of Abbreviations

ABF	Appel, Bockhorn and Frenklach mechanism
CFD	Computational Fluid Dynamics
DNS	Direct Numerical Simulation
DRG	Directed Relation Graph
FAME	Fatty Acid Methyl Esters
HACA	Hydrogen-Abstraction Acetylene-Addition
IME	Instituto de Matemática e Estatística
IPRJ	Instituto Politécnico Do Estado Do Rio De Janeiro
LES	Large Eddy Simulation
PAH	Polycyclic Aromatic Hydrocarbon
PPGEQ	Programa de Pós-Graduação em Engenharia Química
PPGMAp	Programa de Pós-Graduação em Matemática Aplicada
PPGMMAT	Programa de Pós Graduação em Modelagem Matemática
RANS	Reynolds-Averaged Navier–Stokes
UERJ	Universidade do Estado do Rio de Janeiro
UFPEL	Universidade Federal de Pelotas
UFRGS	Universidade Federal do Rio Grande do Sul

List of Symbols

α	Terms of the semi-empirical model
β	Terms of the semi-empirical model
Δ	Smagorinsky model spatial filter
δ	Kronecker delta function
Δt	Time step
$\dot{\omega}$	Source term
ϵ	Rosenbrock method tolerance error
γ	Soot collision efficiency
κ	Terms of the semi-empirical model
λ	Thermal conductivity
μ	Dynamic viscosity
μ_T	Turbulent viscosity
∇	Divergent operator
ν	Stoichiometric coefficient
ω	Reaction rate
ρ	Density
σ	Relaxation coefficient of the density equation
τ	DRG method coefficient
$\mathbf{u}$	Velocity vector

ε	Threshold of the DRG method
Ξ	Local truncation error
A	Frequency factor
A_S	Soot surface area
C_S	Smagorinsky coefficient
c_p	Specific heat at constant pressure
$d; D$	Jet inlet diameters
E_a	Activation energy
G	Mass difusivity
h	Lenght measurements
K	Reaction velocity
L	Lenght measurements
P	Chemical species
p	Pressure
Pr	Prandtl number
Q	Combustion heat
Re	Reynold number
S	Deformation tensor
Sc	Schmidt number
T	Temperature (K)

t	Time
W	Molecular weight
w	Lenght measurements
X	Molar fraction
x, y, z	Position components
Y	Mass fraction
Z	Mixture fraction
Ze	Zel'dovich number

ABSTRACT

Contributions in the study about the generation of pollutants in the combustion of renewable fuels are of great relevance in the current environmental and economic scenario; as it seeks to consolidate the consumption of alternative (bio)fuels to replace non-renewable fuels, such as coal, natural gas and oil. The range of renewable resources, in the short and medium term, used in the production of biofuels has increased significantly, ranging from food crops such as soybeans to biomass from algae. Understanding the combustion process and its effects for these new sources of renewable energy is pertinent to guarantee the quality of the biofuel used and the reduction in emissions of atmospheric pollutants. The objective of this work is to carry out a study on the generation of pollutants, NO_x and soot, after combustion of a biodiesel surrogate, methyl decanoate $-$ MD, with chemical formulation $C_{11}H_{22}O_2$, as works in this direction are scarce in the literature. For this, a turbulent diffusion flame of methyl decanoate was considered, modeled by the equations of CFD - Computational Fluid Dynamics for reactive fluids. The LES - Large Eddy Simulation technique was applied to model the flow turbulence and the Smagorinsky model was adopted for the turbulent viscosity. The equations were discretized by the finite difference method and the system of equations was solved numerically by the Rosenbrock method. To validate the implemented numerical procedure, in addition to the numerical results for turbulent diffusive flames of MD, numerical tests were also carried out for turbulent methanol diffusive flames. The results obtained agree with data found in the literature.

Keywords: Computational Fluid Dynamics; Turbulent jet diffusion flames; Methyl decanoate, NO_x, Soot.

RESUMO

Contribuições nos estudos acerca da geração de poluentes na combustão de combustíveis renováveis são de grande relevância no cenário ambiental e econômico atual; uma vez que se busca consolidar o consumo de (bio)combustíveis alternativos em substituição aos combustíveis de origem não-renováveis, como o carvão mineral, gás natural e o petróleo. A gama de recursos renováveis, a curto e médio prazos, utilizada na produção de biocombustíveis tem aumentado significativamente, indo de culturas alimentares, como soja, até biomassa proveniente de algas. Compreender o processo de combustão e seus efeitos, para estas novas fontes de energias renováveis é pertinente para que se garanta a qualidade do biocombustível utilizado e a redução nas emissões de poluentes atmosféricos. O objetivo deste trabalho é realizar um estudo sobre a geração de poluentes, o NO_x e a fuligem, após a combustão de um substituto do biodiesel, o decanoato de metila $-$ MD, com formulação química $C_{11}H_{22}O_2$, dado que trabalhos nessa direção são escassos na literatura. Para isso, considerou-se uma chama difusiva turbulenta de decanoato de metila, modelada pelas equações da CFD - Dinâmica de Fuidos Computacional para fluidos reativos. Aplicou-se a técnica LES - Large Eddy Simulation para modelar a turbulência do fluxo e o modelo de Smagorinsky foi adotado para a viscosidade turbulenta. As equações foram discretizadas pelo método das diferenças finitas e o sistema de equações foi resolvido numericamente pelo Método de Rosenbrock. Para validação do procedimento numérico implementado, além dos resultados numéricos para chamas difusivas turbulentas de MD, também realizou-se testes numéricos para chamas difusivas turbulentas de metanol. Os resultados obtidos concordam com dados encontrados na literatura.

Palavras-chave: Dinâmica de Fluidos Computacionais; Chama difusiva turbulenta; Decanoato de metila; NO_x; Fuligem.

1 INTRODUCTION

1.1 Motivation

Global power generation has grown significantly in recent decades to supply growing consumer demand. In this context, the use of technologies and studies on clean and renewable energy options has also increased. The attempt to reduce the consumption of fossil fuels is due to the limitation of these non-renewable resources and the concern with environmental pollution rates.

Renewable energy sources comprise energies generated from inexhaustible processes and resources, which are constantly restored in the short or medium term. Some examples are solar, ocean, hydro, wind and biomass energy. Biomass is derived from numerous sources, such as local cultures, animal waste, plants, etc. Biodiesel, specifically, is produced from animal and plant biomass [87] through transesterification [10].

Mathematical modeling of biodiesel combustion is computationally expensive and complex due to the robust structure of biodiesel molecules. An alternative adopted by the researchers is the use of biodiesel substitutes, such as methyl decanoate, for modeling purposes, which has a simpler chemical structure, although maintaining the physicochemical properties of biodiesel.

Combustion may be described mathematically through kinetic chemical mechanisms. Mechanisms with a high number of chemical reactions induce stiff systems of differential equations due to the difference in the reaction time scales of the chemical species [104]. Thus, reduced mechanisms are often used to reduce the system stiffness and, consequently, reduce the computational cost. Smaller mechanisms are advantageous for their prompt response in calculating concentrations of combustion products such as carbon monoxide (CO), carbon dioxide (CO_2), nitric

oxide (NO), nitrogen dioxide (NO_2) and soot. Determining the concentration of these compounds is important whereas they are air pollutants.

The emission of atmospheric pollutants through combustion is a critical factor in choosing the most suitable fuel to be used commercially. Issues in pollutant emission predictions include feedstock, fuel quality, flame configuration, temperature, engine injection timing, ignition timing [71], etc. Fortunately, many practical and theoretical studies have been developed to improve these predictions.

1.2 General Objectives

Numerical modeling and simulation of NO_x and soot formation and oxidation in the study of the combustion of the biodiesel surrogate, methyl decanoate, as a turbulent jet diffusion flame.

1.3 Specific Objectives

- Modeling NO_x and soot formation and oxidation during the combustion of methyl decanoate for different sets of parameters using reduced kinetic mechanisms;

- solve the reactive flow equations for a turbulent jet diffusion flame using the LES technique;

- computationally implement the proposed problem, using suitable numerical solvers for the problem setup;

- analyze the numerical results obtained from simulations of NO_x and soot emissions comparing with data from the literature;

1.4 Structure of the thesis

The Thesis is organized as follows:

- in this chapter, a brief introduction is made about energy conversion through biofuel combustion and pollutant formation; followed by the objectives of this work and finally, the scope of the work;
- in Chapter 2, a literature review on biofuels and pollutants is presented;
- in Chapter 3, the kinetic mechanisms used in the work is presented, as well as the description of the DRG method;
- in Chapter 4, the reactive flow equations and turbulence modeling is described. Afterwards, the equations are formulated dimensionless.
- in Chapter 5, the numerical solvers are shown;
- in Chapter 6, the proposed problem setup is explained;
- in Chapter 7, the numerical results are presented and discussed;
- in Chapter 8, the final considerations about the developed work is reported;
- finally, we list the bibliographical references used in the development of this work.

2 BIOFUELS AND POLLUTANTS

In this chapter we present a theoretical background on biofuel combustion and pollutants. In this study, we emphasize the biodiesel surrogate named methyl decanoate and the main atmospheric pollutants from biodiesel combustion: NO_x, which is a set of nitrogen oxides, and soot, which is composed of solid carbonaceous particles.

The production and consumption of energy has grown exponentially over the years and, consequently, the search for different energy sources has also increased. Choosing alternative energy sources is not simple, as it must consider environmental, economic and social factors.

In 2020, 85.1% of the total energy demand consumed worldwide came from primary resources (coal, natural gas and petroleum), while only $14,9\%$ came from renewable resources. In Brazil, specifically, 51.6% of total energy consumption in the same year came from primary resources and 48.4% from renewable sources [62].

Primary resources are exhaustible sources of energy. In order to replace the excessive consumption of these resources, technologies and scientific studies on alternative and renewable energy sources have been applied. Renewable energy sources comprise energies generated from unlimited processes and resources, which are constantly re-established in short or medium terms; such as solar, ocean, water, wind and biomass energy.

Biomass is derived from organic, raw materials, such as animal residue, agricultural and forestry waste, industrial and urban rubbish and food processing, as well as algae and aquatic plants. Biomass produces energy through direct combustion [87], thermochemical processes: gasification [56], pyrolysis [11] and transesterification [10]; or biological processes: anaerobic digestion [109] or fermentation [105].

Biomass is the leading component for the (bio)fuels production, either in liquid form such as biodiesel, diesel, ethanol and methanol; or gaseous form: biogas, hydrogen and methane. The most used biofuels are ethanol, methanol, biogas and biodiesel [12].

Ethanol (C_2H_5OH) is mostly used as a partial substitute for gasoline. The world's largest ethanol producers are the United States and Brazil. Their annual production in recent years is described in table (2.1) based on data from [86]. First-generation ethanol is produced from the fermentation of carbohydrates (sugars) derived from crops such as corn (the main raw material used in the USA), sugar cane (most used in Brazil), beets, canola, palm, wheat and cassava. In the second generation, residues from the first generation are used, such as sugarcane bagasse, wheat straw, corn and beet residues, etc.

Table 2.1: Annual World Ethanol Production (million gallons).

Region / Year	2018	2019	2020
United States	16,1	15,6	13,9
Brazil	8	8,6	7,9

Methanol (CH_3OH) is a methyl alcohol used in biodiesel production and it is used to replace kerosene in jet aircraft. Methanol is highly flammable and toxic so it is not common to use it in ordinary engines. It is produced from sugarcane processing or wood distillation, such as eucalyptus, or by gasification. In the gasification process, solid biomass is converted into synthesis gas [11] and subsequently transformed into a liquid state.

Biogas is a mixture composed mainly of methane gas (CH_4), carbon dioxide (CO_2) and low amounts of hydrogen sulphide (H_2S), hydrogen (H_2), nitrogen (N_2) and oxygen (O_2). Biogas has similar properties to natural gas. A priori, biogas is formed naturally when the biomass is decomposing under anaerobic circum-

stances, that is, absence of oxygen, such as in animal intestines, swamps and landfills, for example. However, biogas can also be obtained through anaerobic biodigesters, which are equipment designed to capture biogas from the processing of biodegradable organic waste [109].

Biodiesel is intended for transportation means with compression ignition engines (diesel engines), partially replacing conventional diesel. The world's largest biodiesel producers are Indonesia, the United States and Brazil, as reported in [85] and shown in table (2.2).

Table 2.2: Biodiesel production in 2020 (billion liters).

Country	Production in 2020	Global total production
Indonesia	8	17%
United States	6,78	14,4%
Brazil	6,45	13.7%

Biodiesel is a biofuel with a diversified, easily available raw material, economically viable and environmentally acceptable [27]. Biodiesel will be highlighted in this work.

2.1 Biodiesel

Biodiesel is a set of monoalkyl esters of long-chain fatty acids obtained by transesterification [113] in which a triacylglycerol reacts with an alcohol, such as methanol. Acidic or basic catalysts are commonly used in the transesterification process [46, 70], since they accelerate reactions without being consumed. The products obtained from this process are biodiesel and glycerol. Glycerol can be decanted or used in food, pharmaceutical and other industries.

Transesterification reduces the oxygen content and viscosity of the fatty acid, and thus, biodiesel will present physicochemical characteristics similar to those of petroleum diesel. Figure (2.1) illustrates the global transesterification process.

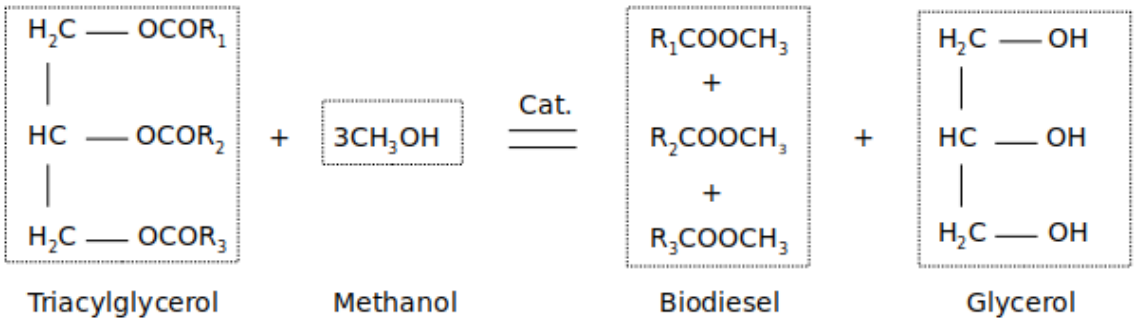

Figure 2.1: Global transesterification process.

Biodiesel comes from a wide variety of biomass. The type of raw material and processing technology used in its production classifies biodiesel into: first generation, second or third generation [30]. First generation biodiesel is produced from oilseeds [46], such as soybeans, palm, cottonseed, peanuts, sunflower, linseed, etc. The production of biodiesel from these crops directly competes with the food market, which is one of the factors behind the high cost of producing first-generation biodiesel. On the other hand, second and third generation biodiesel has made it possible to reduce production costs.

Second-generation biodiesel comes from non-food crops such as rapeseed, jatropha, jojoba and poppy seed; animal waste such as swine fat and beef tallow; or food residues such as waste and frying oils. And finally, third-generation biodiesel is derived from algae and aquatic plants [7].

The main raw material used in the production of biodiesel influences its composition, that is, in the concentrations of each fatty acid. The table (2.3) shows the percentage of fatty acids for biodiesel produced from rapeseed and soybean [41].

Table 2.3: Chemical formulation of the main fatty acids in biodiesel.

Fatty acid methyl esters (FAME)	Chemical formulation	Rapeseed biodiesel	Soy biodiesel
methyl linoleate	$C_{19}H_{34}O_2$	$21,1\%$	$50-60\%$
methyl linolenate	$C_{19}H_{32}O_2$	$13,2\%$	$5-11\%$
methyl oleate	$C_{19}H_{36}O_2$	$59,9\%$	$20-30\%$
methyl palmitate	$C_{17}H_{34}O_2$	$4,3\%$	$6-10\%$
methyl stearate	$C_{19}H_{38}O_2$	$1,3\%$	$2-5\%$

Biodiesel can be used pure or blended with petroleum diesel. Most countries, including Brazil, sell the blend of biodiesel and petroleum diesel as it does not require modifications to diesel engines. Blends are classified according to their percentage of biodiesel, for example, $B5$ represents a blend composed of 5% biodiesel and 95% petroleum diesel, whilst $B20$ represents a blend of 20% biodiesel and 80% conventional diesel.

In Brazil, the sale of blends has been mandatory since 2008, and the percentage of biodiesel in the blend has been gradually increased. Since March 2018, the sale of $B10$ is mandatory, according to Law Nº 13263/16. Currently Resolution Nº 11, of June 2, 2021, establishes the $B12$ mixture as mandatory.

We highlight the following advantages of using biodiesel [46, 80]:

- it is biodegradable and non-toxic as it does not contain aromatics and sulfur in its composition, in addition to being highly oxidizable.
- being an oxygenated fuel, it contributes to complete combustion;
- it has greater combustion efficiency [28] due to the ar−fuel ratio;
- can be used as a lubricating additive as it has a higher viscosity than diesel;

- it does not contain aromatic compounds, reducing pollutant emissions such as particulate matter and soot;

- THC emissions (total hydrocarbons) are lower, as the number of cetanes (which relates the fuel injection time and the start of combustion) is higher;

- it has immediate availability and renewability due to the variety of raw materials that can be used in its production;

- it is non-explosive and non-flammable, which makes it safe to store and transport.

Biodiesel molecules have complex structures and high molecular weight making the study of combustion difficult and computationally expensive. Naik et al. (2011) developed a detailed kinetic mechanism for biodiesel combustion considering two of its main components, methyl oleate and methyl stearate, containing more than 17000 reactions and 3500 chemical species [65].

In order to guarantee results, many researchers have considered smaller structures of fatty acids, named surrogates, which belong to the same class of esters as biodiesel, while presenting simpler chemical formulations. In this such way, the study of the combustion of surrogates becomes computationally viable and it provides theoretical foundations for understanding the combustion of biodiesel [29].

Among some biodiesel substitutes studied for modeling purposes, we highlight [48]: methyl butanoate ($MB{-}C_5H_{10}O_2$), methyl crotonate ($MC{-}C_5H_8O_2$), n-heptane (C_7H_{16}), methyl 9-decenoate ($MD9D-C_{11}H_{20}O_2$) and methyl decanoate ($MD-C_{11}H_{22}O_2$). Methyl decanoate is studied in this work.

2.1.1 Methyl Decanoate

Methyl decanoate is a medium sized methyl ester with 11 carbon atoms. Due to the size of its carbon chain, as illustrated in the Fig. (2.2), MD has been considered the most suitable biodiesel surrogate [89] for the modeling of biodiesel combustion. MD has physicochemical characteristics similar to biodiesel [90]. Furthermore, studies also show that the MD combustion process is kinetically similar to biodiesel combustion [89].

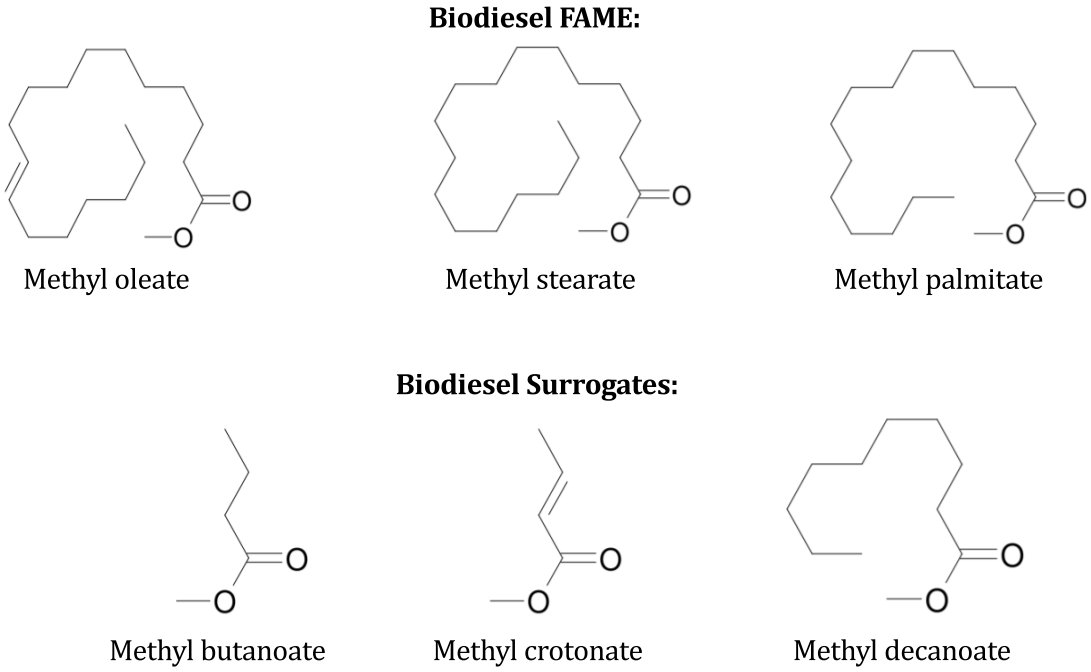

Figure 2.2: Biodiesel FAME and biodiesel surrogates [89].

2.2 Pollutants

Pollutants derived from the (bio)fuels combustion can be defined as chemical compounds generated during oxidation reactions of (bio)fuels. Pollutants cause harmful effects to the environment, ecosystems and humans. Atmospheric pollutants, which can be aerosols, gases or solid particles, are generally classified as: (a) primary: compounds directly emitted into the environment; b) secondary: substances resulting from the oxidation of initiators already existing in the atmosphere. The main air pollutants are CO, CO_2, NO_x, soot, SO_x, HC unburned, O_3 and particulate matter (including soot).

Carbon monoxide (CO) is mainly generated from incomplete combustion, therefore, the oxidant is insufficient for the complete burning of the fuel. It is a gas less dense than air, it is colorless, odorless and flammable [66]. It can easily associate with hemoglobin forming carboxyhemoglobin, which compromises cell oxygenation causing intoxication, asphyxia, convulsion and, in some cases, even death [14, 19].

Carbon dioxide (CO_2) can be generated through the oxidation of CO or complete combustion, that is, when there is enough oxidant to consume the fuel. It is denser than air, colorless, odorless and soluble in water [98]. Carbon dioxide is essential for the photosynthesis process and therefore it makes an important role in the carbon cycle. However, high emission rates of CO_2 cause damage to the environment, such as acid rain, pollution and overheating of the earth, intensifying the greenhouse effect.

The term SO_x refers to several compounds containing sulfur and oxygen, with sulfur dioxide (SO_2) and sulfur trioxide (SO_3) being the most representative of them. The main emitting source of SO_2 is the burning of fossil fuels that contain sulfur in their composition, such as conventional diesel. When released into the environment, some of the SO_2 is oxidized by air and converted to SO_3. SO_2 and

SO_3 are precursors of sulfuric acid (H_2SO_4) and they contribute to the release of sulfate particulate matter and the formation of acid rain. While the emission rates of SO_x from burning diesel are high, biodiesel does not emit SO_x, as it does not have sulfur in its composition [68].

Unburned hydrocarbons (HC) are particles of C_mH_n that have not been consumed in combustion or that have been partially oxidized. The main representatives are methane (CH_4) and total hydrocarbons (THC). Unburned HCs are potential greenhouse gas aggravators, which when reacting with other pollutants, such as NO and NO_2, can form ozone (O_3), thus contributing to the formation of photochemical smog [18]. Photochemical smog is a grayish fog formed by nitrogen oxides, carbon oxides, ozone and other compounds resulting from photochemical reactions carried out between sunlight and pollutant gases released in the combustion of fuels [93]. Reduced visibility and respiratory problems are the main harmful effects of photochemical smog.

Particulate materials (PM) are thin solid fragments with different physicochemical characteristics depending on the emitting source. They can consist of dust, black carbon, pollen and contaminating materials released in combustion activities. Soot is a type of particulate material with a maximum size of $2.5\mu m$, while other types of particulate material can reach a maximum size of $10\mu m$. The main harmful effect of particulate materials is related to human health [3, 91] as the particles can be inhaled, and in this case, they aggravate respiratory problems. In addition, the small size of these particles allows them to pass into the bloodstream, aggravating any heart problems.

2.2.1 NO_x

The term NO_x represents a set of chemical compounds formed from nitrogen and oxygen, described in the table (2.2.1). However, the two most com-

mon gases in this family are nitrogen monoxide (NO) and nitrogen dioxide (NO_2), which are considered primary pollutants [42]. The NO_x is derived from a variety of natural and anthropogenic sources [115], among which the main emitting source is the combustion of (bio)fuels at high temperatures.

The nitrogen and oxygen present in the oxidant, under specific conditions, react with each other during the combustion process, forming mostly NO. Subsequently, the NO is oxidized in the environment contributing to the increase in NO_2 emission rates [69]. Gases are emitted in the troposphere where they are heated by ambient temperature and thus, their densities decrease and the gases migrate to the stratosphere and mesosphere.

Table 2.4: Nomenclature of the chemical species represented by NO_x.

Chemical species	Nomenclature
NO	Nitric oxide
NO_2	Nitrogen dioxide
N_2O	Nitrous oxide
N_2O_2	Hyponitrite
N_2O_3	Dinitrogen trioxide
N_2O_4	Dinitrogen tetroxide
N_2O_5	Dinitrogen pentoxide

NO and NO_2 are both pungent, soluble, and toxic gases. The first gas is colorless and the second gas is brown. The NO is common in human metabolism in small amounts, it dilates the vessels increasing blood flow. In larger amounts, both are harmful to humans, causing lung irritation as well as contributing to respiratory infections such as asthma and bronchitis.

The emissions of NO and NO_2 contribute to the acidification of rainfall and the formation of smog [63]. Furthermore, the release of NO into the environment

also favors the increase of nitrogen in the water, leading to eutrophication (a process in which there is overgrowth of aquatic plants) and harming fauna and flora systems.

Although N_2O is not considered a primary pollutant, Fernando et al. (2006) [34] asserts that N_2O aggravates the greenhouse effect with global warming potential 310 times greater than CO_2.

2.2.2 Soot

Soot is the term commonly used for particulate materials with a maximum diameter of $2.5\mu m$. It is composed of a range of pollutants, such as black carbon particles, NO_x and SO_2, which are dispersed in the environment after their emission. The main sources of soot emission are industrial, petrochemical, residential and vehicular processes.

The formation and oxidation of soot occurs particularly during the incomplete combustion process of hydrocarbon-rich fuels [13] at high temperatures. Parameters such as fuel type, oxidant, fuel flow rates, mixture patterns, temperatures and pressure affect the [72] composition, shape and characteristics of the soot emitted. These factors make the prediction of soot emission complex and in some cases insufficient [22].

Soot formation occurs in five stages [78, 61, 116]: pyrolysis, nucleation, coalescence, surface growth and agglomeration. In pyrolysis, fuel molecules break down and soot starts to form from precursors such as polycyclic aromatic hydrocarbons (PAH). Nucleation is the formation of the nucleus of soot particles in which the particles gain mass and volume [96]. In the coalescing phase and in the surface growth phase, the particles unite to form a larger one, which increase due to the absorption of other residues. Finally, the agglomeration step comprises the union of several particles forming the final three-dimensional structure of the soot [107].

Soot particles absorb solar radiation, contributing to global warming. In addition to promoting the formation of dark colored fogs, which reduces visibility in areas with high emission rates, soot contributes to the acidification of lakes and rivers. Soot is also harmful to human health and can cause worsening of asthma, respiratory infections and even lung cancer [106].

3 KINETIC MECHANISMS

This chapter presents a brief list of reduced or detailed kinetic mechanisms that describe the pyrolysis and oxidation of methyl decanoate as well as the formation and oxidation of NO_x and soot.

Understanding combustion requires understanding the chemical kinetics of reactions that take place in the combustion process. Detailed kinetic mechanisms describe all chemical reactions involved in the ignition process and are important for combustion analysis, development and control.

The high number of elementary reactions of the detailed kinetic mechanism depends on parameters such as reaction rate rates. These rates are complex to determine [50] as they vary according to the type of flame and combustion conditions. Furthermore, reactions can also exhibit highly reactive radicals and several orders of magnitude on time scales. These factors contribute to the stiffness of the system of equations that models the problem [75].

A detailed mechanism for MD combustion was proposed by Herbinet et al (2008) [43]. This mechanism contains 8820 elementary reactions and 3012 chemical species, and it is valid for low and high temperatures. Since then, it has been used as a reference for other MD oxidation mechanisms.

Although the MD mechanism is less than a detailed mechanism for the oxidation of biodiesel, it is still considered computationally prohibitive. It is sought then, through mechanisms of reduction of mechanism, to obtain reduced mechanisms but still with quality.

3.1 Mechanism Reduction Techniques

The systematic reduction of detailed mechanisms has been developed from the 1980s onwards for methane flames using techniques such as steady state and partial equilibrium hypothesis. Currently, these reduced kinetic mechanisms are used in asymptotic and numerical analysis of the combustion process. This methodology is important and valid because it reduces the number of elementary reactions, consequently it reduces the number of parameters and the rigidity of the system of equations. From the systematic reduction it is possible to simplify the modeling and still satisfactorily describe the combustion process maintaining the accuracy of the predictions and in counterbalance, with lower computational effort.

The steady-state hypothesis is applied when the concentration gradient of a chemical species i, represented by X_i, is almost always null, which occurs when the species is consumed faster than it is produced. Then we write

$$\frac{d[X_i]}{dt} = \sum_{p=1}^{m_p} \nu_{ip} w_i \simeq 0, \tag{3.1}$$

where ν_{ip} are the stoichiometric coefficients and w_i is the reaction rate of species i.

For the partial equilibrium hypothesis, it is assumed that certain elementary reactions are in equilibrium, that means, the forward reaction (K_d) and reverse reaction (K_r) velocities are similar, then we write:

$$\frac{K_d - K_r}{K_d + K_r} \approx 0. \tag{3.2}$$

In this way, we write the concentration of reactants and products in terms of their forward and reverse reaction coefficients, decoupling the equations of the system [108]. Nevertheless, the application of the steady-state hypothesis is valid only when reaction rates are high.

Reduced mechanisms are obtained by adequate steady-state or partial equilibrium hypotheses for certain chemical species. It is also possible to disregard

terms and reactions with less influence on the combustion process, in order that the chemical description of the flame structure is simplified [112] but still efficient. Peters (1988) [73, 75] described the steps to apply the systematic reduction method:

- estimation of the order of magnitude of the velocity rates of elementary reactions;
- introduction of the partial equilibrium hypothesis;
- definition of the main chain in the mechanism;
- identification of the main chain reactions and their rates;
- application of the permanent regime hypothesis;
- validation of the reduced mechanism through asymptotic analysis.

Applying this scheme, an effective reduced kinetic mechanism can be obtained for high temperature regimes. Furthermore, one must consider that a certain error (tolerance) of approximation in the system solutions for reduced mechanisms must be accepted [60].

3.1.1 Directed Relation Graph

The Directed Relation Graph (DRG) technique was proposed by Lu et al. (2005) [53] to write skeleton mechanisms from detailed mechanisms. This model studies the coupling level of the species involved in the mechanism and eliminates those considered unimportant, depending on a predetermined threshold [54, 55].

The species coupling analysis considers that two species A and B are strongly coupled directly if they are together in the same reaction, and that they are strongly indirectly coupled if each of them is coupled to a third species C, even if they do not belong to the same reaction.

In this way, when a certain species is removed from the mechanism, it becomes necessary to remove an entire set of species that are strongly coupled to this certain species [53]. And, equally, if a species is kept in the mechanism, then it must also keep all species strongly coupled to it.

Figure (3.1) illustrates a graph that well represents the DRG technique. Consider graph nodes as species of detailed mechanisms and edges as couplings. The edge directed from A to B indicates that these species are directly linked, that means, that the removal of species B implies significant errors in the rate of production/consumption of species A.

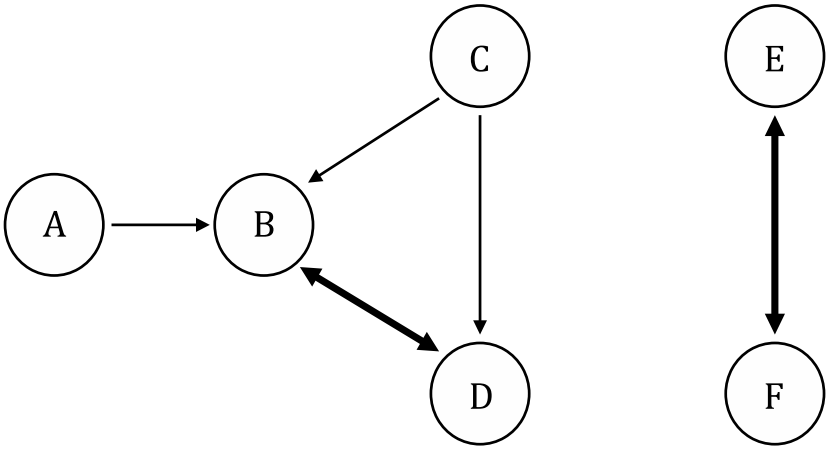

Figure 3.1: Direct Relation Graph Sketch.

Given a mechanism with r elementary reactions, the normalized contribution of species B to the production rate of species A can be calculated by:

$$\tau_{AB} = \frac{\sum_{i=1,r} |\nu_{A,i}\omega_{A,i}\delta_{B,i}|}{\sum_{i=1,r} |\nu_{A,i}\omega_{A,i}|}, \tag{3.3}$$

where i is the ith reaction, $\nu_{A,i}$ is the stoichiometric coefficient of species A in the ith reaction, $\omega_{A,i}$ is the reaction rate and $\delta_{B,i} = 1$, if the ith elementary reaction involves species B, or $\delta_{B,i} = 0$, otherwise.

For a small $0 \leq \varepsilon < 1$ parameter initially defined and considering an important species A, the DRG technique eliminates a species S from the mechanism

if and only if $\tau_{AS} < \varepsilon$. Species A and S are not strongly coupled and species S does not significantly influence the production rate of important species A.

In case $\tau_{AB} \geq \varepsilon$, species A depends on B and we say that B is reachable from A. All species reachable from A forming a set named dependent set of A and denoted by S_A. If species A is kept in the mechanism, then the set S_A is also kept in the mechanism.

Threshold ε influences the number of species to be eliminated from the mechanism and, consequently, the number of reactions in the skeleton mechanism. If ε tends to zero, the skeleton mechanism will be closer to the detailed mechanism. As ε is increased, the skeleton mechanism will be smaller, although, the efficiency and accuracy of the mechanism will also be reduced.

3.2 Kinetic Mechanisms for MD

In order to enable the study of MD combustion, as well as other biodiesel substitutes, several researchers have prioritized the use of reduced, quasi-global or global mechanisms.

Quasi-global or global mechanisms are indicated in the initial flame study, providing information for a limited number of species. The reaction rates, although empirical, approximate the real [23] rates of elementary reactions that describe the combustion process. One of the advantages of using global mechanisms is the reduced computational time, which decreases by the same order of magnitude as the reduction in chemical species of a simplified mechanism.

Global or quasi-global mechanisms satisfactorily approximate the reaction rate for certain flame conditions, in contrast, product concentrations may be overestimated. We describe some examples of global or quasi-global mechanisms for MD combustion:

i) One-step mechanism:

$$C_{11}H_{22}O_2 + 15.5O_2 \longrightarrow 11CO_2 + 11H_2O \tag{3.4}$$

ii) Two-step mechanism:

$$\begin{cases} C_{11}H_{22}O_2 + 10O_2 \rightleftharpoons 11CO + 11H_2O \\ CO + 0.5O_2 \rightleftharpoons CO_2 \end{cases} \tag{3.5}$$

iii) Five-step mechanism:

$$\begin{cases} C_{11}H_{22}O_2 \rightleftharpoons 5.5C_2H_2 + 7H_2 + 2H_2O \\ C_2H_2 \rightleftharpoons 2C_S + H_2 \\ C_S + 0.5O_2 \rightleftharpoons CO \\ C_S + H_2O \rightleftharpoons CO + H_2 \\ H_2 + 0.5O_2 \rightleftharpoons H_2O \end{cases} \tag{3.6}$$

Mechanism (3.4) is simple but provides important information about the four basic species of a system. A disadvantage of the mechanism is that it does not describe the formation of CO and H_2, species significant for combustion and which are in equilibrium with the species CO_2 and H_2O for adiabatic flame temperatures ($\approx 2000K$) [110].

Mechanisms (3.5) and (3.6) provide more accurate information about these species, as well as data about the other species. Mechanism (3.6), adapted from [52], contains the species C_2H_2 which is considered a soot precursor, in addition to C_S, which is carbon in solid form, a species also important for pollutants formation.

iv) 26-step mechanism:

We applied the DRG technique systematically to the kinetic mechanism provided by The CRECK Modeling Group [37, 82, 83, 81] and we obtained the reduced mechanism for MD oxidation described in Table (3.1). The mechanism includes the

MD molecule split and the formation and oxidation of species such as C_2H_2, C_2H_3 and OH, considered as soot precursors. Kinetic parameters, thermodynamic and transport properties are provided by The CRECK Modeling Group [32] and they were adjusted for the fuel used in this work.

Table 3.1: Simplified Mechanism for MD. Units are mol, cm^3, s, K and cal/mol.

No.	Reactions	A	b	E_a
1	$H_2 + M = 2H + M$	$4.5770e+19$	-1.400	104400.00
2	$H_2 + O = H + OH$	$5.0800e+04$	2.670	6292.00
3	$H_2 + OH = H + H_2O$	$4.3800e+13$	0.000	6990.00
4	$H + O_2(+M) = HO_2(+M)$	$4.6500e+12$	0.440	0.00
5	$H_2 + OH = H + H_2O$	$4.3800e+13$	0.000	6990.00
6	$O + H_2O = 2OH$	$6.7000e+07$	1.704	14986.80
7	$H + O_2 = O + OH$	$1.1400e+14$	0.000	15286.00
8	$OH + HO_2 = O_2 + H_2O$	$7.0000e+12$	0.000	-1092.96
9	$2HO_2 = O_2 + H_2O_2$	$1.9000e+11$	0.000	-1408.92
10	$OH + CO = H + CO_2$	$7.0150e+04$	2.053	-355.70
11	$HCO + M = H + CO + M$	$5.7000e+11$	0.660	14870.00
12	$H + HCO = H_2 + CO$	$7.3400e+13$	0.000	0.00
13	$OH + HCO = H_2O + CO$	$3.0110e+13$	0.000	0.00
14	$O_2 + CH_2(S) = H + OH + CO$	$2.8000e+13$	0.000	0.00
15	$OH + CH_2O = H_2O + HCO$	$7.8200e+07$	1.630	-1055.00
16	$HO_2 + CH_3 = O_2 + CH_4$	$1.1600e+05$	2.230	-3022.00
17	$O + C_2H_2 = CO + CH_2$	$7.3950e+08$	1.280	2472.00
18	$H + C_2H_2(+M) = C_2H_3(+M)$	$1.7100e+10$	1.266	2709.00
19	$OH + C_2H_4 = H_2O + C_2H_3$	$2.2300e+04$	2.745	2215.50
20	$O_2 + C_3H_5 = HO_2 + C_3H_4$	$4.9900e+15$	-1.400	22428.00
21	$CH_3 + C_3H_6 = CH_4 + C_3H_5$	$1.3480e+00$	3.500	12850.00
22	$C_4H_6O_2 = CO_2 + CH_3 + C_2H_3$	$2.0000e+16$	0.000	85000.00
23	$NC_5H_{11} = CH_4 + C_3H_6 + CH$	$3.3000e+13$	0.000	30000.00
24	$NC_7H_{15} = C_2H_4 + NC_5H_{11}$	$6.2000e+12$	0.000	30000.00
25	$HO_2 + NC_7H_{16} = H_2O_2 + NC_7H_{15}$	$9.6000e+06$	2.000	16000.00
26	$MD = NC_7H_{16} + C_4H_6O_2$	$2.0000e+16$	0.000	85000.00

In this work, we used all the mechanisms mentioned for MD oxidation, as we improved the precision of the results.

3.3 Kinetic Mechanisms for NO_x

The formation of NO_x during the ignition of biofuels whose composition does not contain nitrogen (N_2) is generally described by four kinetic mechanisms, which use the N_2 present in the oxidant.

3.3.1 Thermal Mechanism

Zel'dovich et al. (1947) [114] proposed a mechanism of nitrogen oxidation and, consequently, the formation of NO_x described by the reactions:

$$\begin{cases} I) & O + N_2 & \rightleftharpoons & N + NO \\ II) & N + O_2 & \rightleftharpoons & O + NO \end{cases} \tag{3.7}$$

Including the third reaction described by:

$$III) \quad N + OH \rightleftharpoons H + NO, \tag{3.8}$$

we have the extended Zel'dovich mechanism.

The thermal mechanism is suitable for systems with temperatures above $1800K$ [103] and it is valid for many oxidizer-fuel ratios. The reaction parameters of the Zel'dovich mechanism given in Table (3.2) are used in the Modified Arrhenius Equation:

$$K = AT^b exp\left(- \frac{E_a}{RT} \right), \tag{3.9}$$

where A represents the frequency factor, T is the temperature and b is its exponent, E_a is the activation energy and R is the universal gas constant.

The MD combustion mechanism and the NO_x formation mechanism are coupled by the species O and OH. However, the biofuel oxidation kinetics is faster than the NO_x formation kinetics by the Zel'dovich mechanism. Thus, the largest percentage of NO is formed after combustion, therefore both mechanisms

Table 3.2: Kinetic parameters of the extended Zel'dovich mechanism. Units are mol, cm^3, s, K and cal/mol.

Reactions	A	b	E_a/R
I_f	1.8×10^{11}	0	38370
I_b	3.8×10^{10}	0	425
II_f	1.8×10^{7}	1	4680
II_b	3.8×10^{6}	1	20820
III_f	7.1×10^{10}	0	450
III_b	1.7×10^{11}	0	24560

can be modeled separately. The mass fractions of N_2, O_2 and OH are assumed to be equal to their equilibrium values obtained from the full combustion.

For the two-step Zel'dovich mechanism, we assume that the reaction II is faster than the reaction I, and we also assume that the species N is in steady state. Thus, the equation of the NO formation rate can be given by [45]:

$$\frac{d[NO]}{dt} = 2[O]\left\{ \frac{K_{I_f} K_{II_f} [O_2][N_2] - K_{I_b} K_{II_b} [NO]^2}{K_{II_f}[O_2] + K_{I_b}[NO]} \right\}. \tag{3.10}$$

The concentrations of O along the flame region assume low values making their calculation difficult. To approximate the values of the mass fraction of O, the equation proposed by Westenberg [111] is:

$$[O] = AT^b [O_2]^{0.5} exp\left(\frac{E}{RT}\right). \tag{3.11}$$

The rates of the equation (3.11) were experimentally determined in [42, 79] and, in particular, Jiang et al. (2006) [45] proposed the equation:

$$[O] = 12.2T^{0.52} [O_2]^{0.5} exp\left(\frac{-29330}{T}\right). \tag{3.12}$$

3.3.2 Fenimore Mechanism

Fenimore (1971) [33] described the NO_x prompt mechanism, in which NO is formed by reactions between hydrocarbons and molecular nitrogen. The interaction between these species generates amines and cyanides, which are transformed into intermediate compounds such as hydroxyl (OH) and carbon monoxide (CO), and finally converted to NO. The NO_x prompt mechanism consists of the reactions:

$$\begin{cases} I) & CH + N_2 & \rightleftharpoons & HCN + N \\ II) & C + N_2 & \rightleftharpoons & CN + N \\ III) & HCN + O & \rightleftharpoons & NCO + H \\ IV) & NCO + H & \rightleftharpoons & NH + CO \\ V) & NH + H & \rightleftharpoons & N + H_2 \\ VI) & N + OH & \rightleftharpoons & NO + H\ . \end{cases} \tag{3.13}$$

This mechanism describes the formation of NO at the start of combustion since the rates have a higher velocity than the Zel'dovich mechanism. The contribution of the NO_x prompt to the generation of NO is generally small for premixed and non-premixed combustion. However, the mechanism is relevant in the total emission of NO in fuel-rich systems with lower temperatures [92].

3.3.3 N_2O-intermediate Mechanism

Malt & Pratt (1974) [58] presented a valid mechanism for low temperature and oxygen rich systems, which determines the formation of NO_x of the species N_2 using nitrous oxide (N_2O) as an intermediary. The mechanism is described by the reactions:

$$\begin{cases} I) & O + N_2 + M & \rightleftharpoons & N_2O + M \\ II) & O + N_2O & \rightleftharpoons & NO + NO, \end{cases} \tag{3.14}$$

where M is a radical.

The reaction rates of the mechanism are shown in Table (3.3). The rate of formation of NO_x of this mechanism is given by the equation:

$$\frac{d[NO]}{dt} = 2\Big\{K_{II_f}[N_2O][O] - K_{II_b}[NO]^2\Big\}; \tag{3.15}$$

where the concentration values N_2O along the flame are defined by:

$$[N_2O] = \frac{K_{I_f}[N_2][O][M] + K_{II_b}[NO]^2}{K_{I_b}[M] + K_{II_f}[O]}. \tag{3.16}$$

Table 3.3: Kinetic parameters of the N_2O-intermediate mechanism. Units are $mol,\ cm^3,\ s,\ K$ and cal/mol.

Reactions	A	b	E_a/R
I_f	4.4×10^{32}	-8.358	28234
I_b	4×10^{8}	0	28234
II_f	2.9×10^{7}	0	11651
II_b	1.45×10^{-29}	9259	11651

3.3.4 NNH Mechanism

Bozzelli & Dean (1995) [16] suggested a mechanism for the formation of NO applicable to the combustion of hydrogen or hydrocarbons with a high coefficient of carbon and hydrogen. The reaction between fuel and nitrogen generates the radical NNH which, when oxidized, is converted to NO. The following two reactions form the NO formation path through the NNH mechanism:

$$\begin{cases} I) & N_2 + H \rightleftharpoons NNH \\ II) & NNH + O \rightleftharpoons NH + NO\ . \end{cases} \tag{3.17}$$

In this work, the thermal and N_2O-intermediate mechanisms were used.

3.4 Kinetic Mechanisms for Soot

Due to the heterogeneity of soot characteristics, for different fuels and burning conditions, there is no universal theory in the literature about its formation [47]. Several models for soot formation have been developed in recent years, considering aspects of interest to the study.

The numerical approach to predicting soot emission depends on factors taken into account by the researchers. While some models describe all the steps of local soot formation and oxidation, others emphasize the spatial distribution of soot particles, or even the particle size/volume depending on its agglomeration.

3.4.1 C_2H_2-intermediate Model

Kronenburg et al. (2000) [47] described a reduced mechanism for the soot production from a particular hydrocarbon, acetylene (C_2H_2). The mechanism is described below:

$$\begin{cases} I) & C_2H_2 & \rightleftharpoons & 2C_S + H_2 \\ II) & C_S + 0.5O_2 & \rightharpoonup & CO \\ III) & C_S + OH & \rightharpoonup & CO + H. \end{cases} \tag{3.18}$$

The authors considered that the formation and growth of soot derives from the breakage of the C_2H_2 molecule, as defined in reaction I, while the oxidation occurred by the reaction with O_2 and OH, as indicated in reactions II and III in (3.18).

The reaction rates of this mechanism are approximated by:

$$\begin{cases} \overline{K}_{I,f} & = K_{I,d}\ [C_2H_2], \\ \overline{K}_{I,b} & = K_{I,r}\ [C_2H_2]A_S, \\ \overline{K}_{II,f} & = K_{II,d}\ [O_2]A_S, \\ \overline{K}_{III,f} & = K_{III,d}\ [OH]A_S, \end{cases} \tag{3.19}$$

where K is the Arrhenius equation, defined in (3.9). The reaction rate parameters are described in the table (3.4), and A_S is the soot surface area, calculated by [51]:

$$A_S = \left[36\pi\rho N_S \left(\frac{\rho Y_{C_S}}{\rho_S}\right)^2\right]^{1/3}, \tag{3.20}$$

where Y_{C_S} is the soot mass fraction and N_S is the particle number density, presented in Ref. [47].

Table 3.4: Kinetic parameters of the soot formation mechanism by [47]. Units are $mol,\ cm^3,\ s,\ K$ and cal/mol.

Reactions	A	b	E_a/R
I_f	0.63×10^4	0	21000
I_b	0.75×10^3	0	12100
II_f	7.15×10^2	0.5	19800
III_f	0.36	0.5	0

The soot production rate in this mechanism is given by:

$$\frac{dY_{C_S}}{dt} = \left\{2\big(\overline{K}_{I,d} + \overline{K}_{I,r}\big) - \big(\overline{K}_{II,d} + \overline{K}_{III,d}\big)\right\} Y_{C_S}. \tag{3.21}$$

3.4.2 Semi-empirical Model

Cai et al. (2016) [21] proposed a semi-empirical model for predicting soot from two equations, describing the soot volume fraction (ρY_S) and soot particle

number density (N_S). The authors considered four phases of soot formation: inception, growth, coagulation and oxidation. The initiation and growth of soot particles increase the volume fraction, while coagulation and oxidation decrease it.

The authors adopted the soot formation and oxidation mechanism proposed by Appel et al. (2000) [4], named ABF mechanism, which describes the formation of soot precursors through the process of H-abstraction-C_2H_2-addition (HACA) process.

The semi-empirical model equations are defined by:

$$\begin{cases} \dfrac{d(\rho Y_S)}{dt} = \alpha_1 + \alpha_2 - \alpha_4, \\ \dfrac{d(N_S)}{dt} = \beta_1 - \beta_3, \end{cases} \tag{3.22}$$

where α_1, α_2, α_4, β_1 and β_3 are source terms. The index 1, 2, 3 and 4 represent the steps of inception, growth, coagulation and oxidation, respectively.

The C_2H_3 species was considered important for the soot particle inception, therefore it was defined:

$$\begin{aligned} \alpha_1 &= L_{\alpha_1} \times exp(-E_{\alpha_1}/T) \times \rho \times Y_{C_2H_3}, \\ \beta_1 &= \frac{\alpha_1}{W_{C_2H_3} \times C_n}, \end{aligned} \tag{3.23}$$

were $W_{C_2H_3}$ is the C_2H_3 molecular mass and $C_n = 12$ is the number of carbon atoms in the initial soot particle.

The C_2H_2 species influences the surface growth of soot particles, as it chemically binds to other soot precursor species. The soot particle growth term is defined by:

$$\alpha_2 = L_{\alpha_2} \times exp(-E_{\alpha_2}/T) \times \sqrt{A_S} \times \rho \times Y_{C_2H_2}, \tag{3.24}$$

where S is the soot surface area, given by:

$$A_S = \pi N_S \left(\frac{6\rho Y_S}{\pi \rho_S N_S} \right)^{2/3}, \tag{3.25}$$

in which $\rho_s = 1.8\ g/cm^3$ is the soot particle density.

During coagulation, the soot particles agglomerate and, consequently, the soot number density is reduced. On the other hand, coagulation does not affect the soot volume fraction. The term of coagulation is defined as:

$$\beta_3 = 2,25 \times 10^{15} \times T^{1/2} \times N_S. \tag{3.26}$$

The term α_4, which represents the oxidation of soot particles, is composed of two parts that describe the oxidation by O_2 and OH. Both of these oxidation routes are usual for any type of fuel and it is expected that the concentrations of O_2 and OH are higher in oxygenated biofuels, such as MD.

The oxidation by O_2 is defined by:

$$\alpha_{4,O_2} = L_{\alpha_{4,O_2}} \times \frac{12 \times A_S}{M_s}\left[\frac{K_A P_{O_2}}{1 + KZP_{O_2}}x + K_B P_{O_2}(1-x)\right], \tag{3.27}$$

where M_s is the molecular mass of one carbon atom, P_{O_2} is the partial pressure of oxygen and

$$\begin{cases} x & = \dfrac{P_{O_2}}{P_{O_2} + K_T/K_B}, \\ K_A & = 30 \times exp(-15800/T), \\ K_B & = 8 \times 10^{-3} \times exp(-7640/T), \\ K_T & = 1.51 \times 10^5 \times exp(-49800/T), \\ K_Z & = 27 \times exp(3000/T). \end{cases} \tag{3.28}$$

The oxidation by OH is expressed as:

$$\alpha_{4,OH} = L_{\alpha_{4,OH}} \times \gamma_{OH} \times \chi_{OH} \times T^{-1/2} \times A_S \times exp(-19023/T), \tag{3.29}$$

where $\gamma_{OH} = 0.1$ represents the collision efficiency between the soot particle and the radical OH and χ_{OH} is the molar fraction of OH.

The parameters L_{α_1}, L_{α_2}, $L_{\alpha_{4,O_2}}$, $L_{\alpha_{4,OH}}$, E_{α_1} and E_{α_2} were reported in [21]. They were chosen from a sensitivity study and varying these parameters

softens or accentuates the peak soot volume fraction, and some combinations of parameters significantly alter the volume fraction gradients.

4 METHODOLOGY

In this chapter, we present the mixture fraction equations and species conservation equations that describe the reactive characteristic of the burning fluid. We incorporate these equations to the classic Navier-Stokes equations: conservation of mass, specific density, momentum and temperature. Therefore, we fully describe the reactive flow, both in laminar and turbulent conditions. In this work, we will use the dimensionless version of the equations.

4.1 Mixture Fraction

A chemical species is a combination of chemical elements. For example, methane (CH_4) is formed by one atom of carbon (C) and four atoms of hydrogen (H). CH_4 is called a species while C and H are elements.

According to Lavoisier's law of mass conservation, both mass and chemical elements are conserved during chemical reactions in a closed system. This means that in a chemical reaction, the species interact with each other rearranging their elements to form other species. All elements are preserved. The mass of chemical elements does not vary, but as chemical species change into others, the mass of species varies.

We can quantitatively describe the chemical transformation between species based on their concentration ratios, either in terms of their moles or mass number. A system with n chemical species contains a large number of molecules, where $6,0236.10^{23}$ molecules is called one mole. The molar fraction of a chemical species is defined by:

$$X_i = \frac{n_i}{n_s} = \frac{n_i}{\sum_{i=1}^{n} n_i,};\ i = 1, 2, \ldots, n; \tag{4.1}$$

where n_i is the number of moles of the species i and n_s is the total number of moles.

The mass fraction of a species i is given by:

$$Y_i = \frac{m_i}{m} = \frac{W_i n_i}{\sum_{i=1}^{n} m_i}, \quad i = 1, 2, \ldots, n; \tag{4.2}$$

where m_i is the mass of all molecules of the species i, W_i is the molecular weight of the species i and m is the total mass of the molecules in the system.

The following equation lists the molar fraction (X_i), mass fraction (Y_i) and concentrations ($[X_i]$) of chemical species:

$$[X_i] = \frac{\rho}{W} X_i = \frac{\rho}{W_i} Y_i, \tag{4.3}$$

where ρ is the specific density and W is the average molecular weight, defined as:

$$W = \sum_{i=1}^{n} W_i X_i = \left(\sum_{i=1}^{n} \frac{Y_i}{W_i} \right)^{-1}. \tag{4.4}$$

The mass fraction of chemical elements is important to the study of combustion and will be used later in this work. Let a_{ij} be the number of atoms of the element j contained in the chemical species i, then the mass m_j of all atoms of the element j of the system is now defined:

$$m_j = \sum_{i=1}^{n} \frac{a_{ij} W_j}{W_i} m_i, \tag{4.5}$$

where W_j is the molecular weight of the element j and W_i is the molecular weight of the species i.

Analogously to the equation (4.2), the mass fraction of the element j is defined by:

$$Z_j = \frac{m_j}{m} = \sum_{i=1}^{n} \frac{a_{ij} W_j}{W_i} Y_i, \quad j = 1, \ldots, n_e; \tag{4.6}$$

where n_e is the total number of elements in the system.

A one-step mechanism can be written simply in the form:

$$\sum_{i=1}^{n} \nu_i' X_i = \sum_{i=1}^{n} \nu_i'' X_i. \tag{4.7}$$

The stoichiometric coefficient defined by $\nu_i = \nu_i'' - \nu_i'$ is negative for reactants and positive for products. Similarly, a mechanism with r elementary reactions can be written as

$$\sum_{i=1}^{n} \nu_{ik} X_i = 0, \;\; k = 1, \ldots, r; \tag{4.8}$$

where ν_{ik} is the stoichiometric coefficient of the species i in the reaction k.

Stoichiometry guarantees that the quantities of each element are maintained, according to Lavoisier's law, and thus, the variations of the mass fractions of any two species R_1 and R_2 follow the rule:

$$\frac{dY_{R_1}}{\nu_{R_1} W_{R_1}} = \frac{dY_{R_2}}{\nu_{R_2} W_{R_2}}. \tag{4.9}$$

In a global one-step reaction where the reactants are the oxygenated fuel represented by F and the oxidizer O_2, we have:

$$\frac{dY_F}{\nu_F W_F} = \frac{dY_{O_2}}{\nu_{O_2} W_{O_2}}. \tag{4.10}$$

Integrating the equation (4.10) with respect to time between the initial unburnt state and any later state, we have

$$\frac{Y_{O_2} - Y_{O_2,u}}{\nu_{O_2} W_{O_2}} = \frac{Y_F - Y_{F,u}}{\nu_F W_F}, \tag{4.11}$$

which is rewritten as:

$$\nu Y_F - Y_{O_2} = \nu Y_{F,u} - Y_{O_2,u}, \tag{4.12}$$

where ν is the stoichiometric mass ratio defined as:

$$\nu = \frac{\nu_{O_2} W_{O_2}}{\nu_F W_F}. \tag{4.13}$$

During the ignition process of a diffusion flame, the fuel and the oxidant are initially separated and, when released into the same environment, they mix by convection and diffusion at the molecular level.

Considering a homogeneous system with two jet feeders, in which the mass of the fuel stream is $\dot{m}_1$ and the mass of the oxidant stream is $\dot{m}_2$, we define the fuel mass fraction in the fuel-oxidant mixture as the mixture fraction Z represented by:

$$Z = \frac{\dot{m}_1}{\dot{m}_1 + \dot{m}_2}. \tag{4.14}$$

At a time prior to fuel ignition, the mass fractions of fuel and oxidant can be given as a function of the mixture fraction [74]:

$$Y_{F,u} = Y_{F,1} Z, \tag{4.15}$$

$$Y_{O_2,u} = Y_{O_2,2}(1 - Z); \tag{4.16}$$

where $Y_{F,1}$ and $Y_{O_2,2}$ represent the fuel mass fraction (F) and oxidant mass fraction (O_2) in the initial free stream of fuel (index 1) and oxidant (index 2), respectively.

Substituting (4.15) and (4.16) into (4.12), we obtain the mixture fraction as a function of the mass fractions of the fuel and the reactant (F and O_2):

$$Z = \frac{\nu Y_F - Y_{O_2} + Y_{O_2,2}}{\nu Y_{F,1} + Y_{O_2,2}}. \tag{4.17}$$

A fuel-oxidant mixture is called stoichiometric when its concentrations are in ideal proportions, that is, $\nu Y_F = Y_{O_2}$. Then, the stoichiometric mixture fraction (Z_{st}) is defined as:

$$Z_{st} = \frac{Y_{O_2,2}}{\nu Y_{F,1} + Y_{O_2,2}} = \left(1 + \frac{\nu Y_{F,1}}{Y_{O_2}}\right)^{-1}. \tag{4.18}$$

4.1.1 Burke-Schumann Solution

If $Z < Z_{st}$, the mixture is considered lean, since the concentration of fuel in the mixture is less than the concentration of oxidant, and thus combustion ends when the fuel is entirely consumed; hence, $Y_F = 0$. Meanwhile, the oxidant

mass fraction is determined from the equation (4.12):

$$\nu Y_F - Y_{O_2} = \nu Y_{F,u} - Y_{O_2,u}, \tag{4.19}$$

$$\Rightarrow Y_{O_2} = Y_{O_2,u} - \nu Y_{F,u}, \tag{4.20}$$

$$\Rightarrow Y_{O_2} = Y_{O_2,u} - \nu Y_{F,1} Z. \tag{4.21}$$

The stoichiometric mixture fraction, displayed in equation (4.18), can be rewritten as:

$$Z_{st}\big(\nu Y_{F,1} + Y_{O_2,2}\big) = Y_{O_2,2}, \tag{4.22}$$

$$\Rightarrow \nu Y_{F,1} Z_{st} = Y_{O_2,2}(1 - Z_{st}), \tag{4.23}$$

$$\Rightarrow \nu Y_{F,1} = Y_{O_2,2}\frac{(1 - Z_{st})}{Z_{st}}. \tag{4.24}$$

Replacing equations (4.16) and (4.24) into (4.21), we have the oxidant mass fraction after combustion process:

$$Y_{O_2} = Y_{O_2,2}(1 - Z) - Y_{O_2,2} Z \frac{(1 - Z_{st})}{Z_{st}}, \tag{4.25}$$

$$\Rightarrow Y_{O_2} = Y_{O_2,2}\left(1 - \frac{Z}{Z_{st}}\right). \tag{4.26}$$

For hydrocarbons ($C_m H_n$) and oxygenated fuels ($C_m H_n O_p$), we can write the mass fraction of the elements with respect to reactants before combustion (unburnt state, which is represented by the subindex u) or using the combustion products (burnt state, with no subindex). Thus for the global one-step mechanism

$$\nu_F C_m H_n O_p \; + \; \nu_{O_2} O_2 \; \longrightarrow \; \nu_{CO_2} CO_2 \; + \; \nu_{H_2O} H_2O, \tag{4.27}$$

we have the following equations for the mass fractions of the elements:

- carbon:

$$Z_C = m\frac{W_C}{W_F} Y_{F,u} \quad \text{and} \quad Z_C = m\frac{W_C}{W_F} Y_F + \frac{W_C}{W_{CO_2}} Y_{CO_2}; \tag{4.28}$$

- hydrogen:

$$Z_H = n\frac{W_H}{W_F}Y_{F,u} \quad \text{and} \quad Z_H = n\frac{W_H}{W_F}Y_F + 2\frac{W_H}{W_{H_2O}}Y_{H_2O}; \tag{4.29}$$

- oxygen:

$$Z_O = Y_{O_2,u} \quad \text{and} \quad Z_O = 2\frac{W_O}{W_{O_2}}Y_{O_2} + 2\frac{W_O}{W_{CO_2}}Y_{CO_2} + \frac{W_O}{W_{H_2O}}Y_{H_2O}. \tag{4.30}$$

Considering that after combustion $Y_F = 0$ both equations in (4.28) are equaled and then, taking $Y_{CO_2,st} = m\frac{W_{CO_2}}{W_F}Y_{F,1}Z_{st}$, we have:

$$Y_{CO_2} = Y_{CO_2,st}\frac{Z}{Z_{st}}. \tag{4.31}$$

Performing the same process for the pairs of equations in (4.29) and taking $Y_{H_2O,st} = \frac{n}{2}\frac{W_{H_2O}}{W_F}Y_{F,1}Z_{st}$, we have:

$$Y_{H_2O} = Y_{H_2O,st}\frac{Z}{Z_{st}}. \tag{4.32}$$

If $Z > Z_{st}$, which means there is more fuel than oxidant, the mixture is considered rich. In this case, combustion ends when the oxidant ends, that is, $Y_{O_2} = 0$. Meanwhile, the fuel mass fraction is obtained from (4.12), (4.15) and (4.16), rewritten as:

$$\nu Y_F = \nu Y_{F,1}Z - Y_{O_2,2}(1 - Z). \tag{4.33}$$

The equation of the stoichiometric mixture fraction (4.18) can also be rewritten as:

$$Z_{st}\big(\nu Y_{F,1} + Y_{O_2,2}\big) = Y_{O_2,2}, \tag{4.34}$$

$$\Rightarrow \nu Y_{F,1} = Y_{O_2,2}\frac{(1 - Z_{st})}{Z_{st}}, \tag{4.35}$$

$$\Rightarrow Y_{O_2,2} = \frac{\nu Y_{F,1}Z_{st}}{1 - Z_{st}}. \tag{4.36}$$

$$\tag{4.37}$$

Implementing the equation (4.37) into (4.33), we have the fuel mass fraction after combustion:

$$Y_F = Y_{F,1}\left(\frac{Z - Z_{st}}{1 - Z_{st}}\right). \tag{4.38}$$

Therefore, the mass fractions of CO_2 and H_2O are given by:

$$Y_{CO_2} = Y_{CO_2,st}\left(\frac{1 - Z}{1 - Z_{st}}\right), \tag{4.39}$$

$$Y_{H_2O} = Y_{H_2O,st}\left(\frac{1 - Z}{1 - Z_{st}}\right), \tag{4.40}$$

where $Y_{CO_2,st} = m\dfrac{W_{CO_2}}{W_F}Y_{F,1}Z_{st}$ and $Y_{H_2O,st} = \dfrac{n}{2}\dfrac{W_{H_2O}}{W_F}Y_{F,1}Z_{st}$.

In general, the Burke-Schumann solution determines the mass fractions of the chemical species involved in the global one-step mechanism of a reaction for hydrocarbons and oxygenated fuels combustion in terms of the mixture fraction Z. In summary, we have the following equations:

- before combustion:

$$\begin{cases} Y_{F,u} &= Y_{F,1}Z; \\ Y_{O_2,u} &= Y_{O_2,2}(1 - Z); \end{cases} \tag{4.41}$$

- after combustion:

If $Z < Z_{st}$:

$$\begin{cases} Y_F &= 0; \\ Y_{O_2} &= Y_{O_2,2}\left(1 - \dfrac{Z}{Z_{st}}\right); \\ Y_{CO_2} &= Y_{CO_2,st}\dfrac{Z}{Z_{st}}; \\ Y_{H_2O} &= Y_{H_2O,st}\dfrac{Z}{Z_{st}}. \end{cases} \tag{4.42}$$

If $Z \geq Z_{st}$:

$$\begin{cases} Y_F &= Y_{F,1}\left(\dfrac{Z - Z_{st}}{1 - Z_{st}}\right); \\ Y_{O_2} &= 0; \\ Y_{CO_2} &= Y_{CO_2,st}\left(\dfrac{1 - Z}{1 - Z_{st}}\right); \\ Y_{H_2O} &= Y_{H_2O,st}\left(\dfrac{1 - Z}{1 - Z_{st}}\right); \end{cases} \tag{4.43}$$

where $Y_{CO_2,st} = m\dfrac{W_{CO_2}}{W_F}Y_{F,1}Z_{st}$ and $Y_{H_2O,st} = \dfrac{n}{2}\dfrac{W_{H_2O}}{W_F}Y_{F,1}Z_{st}$.

The Burke-Schumann solution includes an equation for temperature. The first law of thermodynamics characterizes the energy conservation law applied to thermodynamics, describing the balance between different forms of energy, such as internal energy (e), work (w), heat (q) and enthalpy (h). We consider that

$$e = q + w \tag{4.44}$$

$$\Rightarrow de = dq + dw. \tag{4.45}$$

On the other hand,

$$h = e + pv \tag{4.46}$$

$$\Rightarrow dh = de + vdp + pdv \tag{4.47}$$

$$\Rightarrow de + pdv = dh - vdp, \tag{4.48}$$

where p is the pressure and v is the system specific volume.

Therefore, for constant volumes, $dh - vdp = dq + dw$.

In an adiabatic system ($dq = 0$) with constant pressure ($dp = 0$) whose work performed can be neglected ($dq = 0$), we have:

$$dh = 0 \tag{4.49}$$

$$\Rightarrow \int_u^b dh = 0 \tag{4.50}$$

$$\Rightarrow h_b - h_u = 0 \tag{4.51}$$

$$\Rightarrow h_b = h_u. \tag{4.52}$$

In a multicomponent system, the specific enthalpy is the sum of the enthalpies by the weighted masses of the species quantities: $h = \sum_{i=1}^{n} Y_i h_i$. Thus,

$$\sum_{i=1}^{n} Y_{i,b} h_{i,b} = \sum_{i=1}^{n} Y_{i,u} h_{i,u}. \tag{4.53}$$

We can relate the temperature and specific enthalpy through the expression:

$$h_i = h_{i,ref} + \int_{T_{ref}}^{T} c_{p_i} dT, \tag{4.54}$$

where c_{p_i} is the specific heat capacity at constant pressure.

This way, we defined:

$$\sum_{i=1}^{n} Y_{i,b} \left(h_{i,ref} + \int_{T_{ref}}^{T_b} c_{p_i,b} dT \right) = \sum_{i=1}^{n} Y_{i,u} \left(h_{i,ref} + \int_{T_{ref}}^{T_u} c_{p_i,u} dT \right) \tag{4.55}$$

$$\Rightarrow \sum_{i=1}^{n} \left(Y_{i,b} - Y_{i,u} \right) = \int_{T_{ref}}^{T_b} c_{p_i,b} dT - \int_{T_{ref}}^{T_u} c_{p_i,u} dT. \tag{4.56}$$

The specific heat of the mixture is calculated from the mass fraction of the species in the unburnt and burnt state, defined as:

$$c_{p,u} = \sum_{i=1}^{n} c_{p_i}(T) Y_{i,u}; \tag{4.57}$$

$$c_{p,b} = \sum_{i=1}^{n} c_{p_i}(T) Y_{i,b}. \tag{4.58}$$

Considering a global one-step mechanism, equation (4.9) results in:

$$\left(Y_{i,u} - Y_{i,b} \right) = \left(Y_{F,u} - Y_{F,b} \right) \frac{\nu_i W_i}{\nu_F W_F} \tag{4.59}$$

$$\Rightarrow \sum_{i=1}^{n} h_{i,ref}\big(Y_{i,u} - Y_{i,b}\big) = \sum_{i=1}^{n} h_{i,ref}\big(Y_{F,u} - Y_{F,b}\big)\frac{\nu_i W_i}{\nu_F W_F} \tag{4.60}$$

$$\Rightarrow \sum_{i=1}^{n} h_{i,ref}\big(Y_{i,u} - Y_{i,b}\big) = \frac{\big(Y_{F,u} - Y_{F,b}\big)}{\nu_F W_F}\sum_{i=1}^{n} h_{i,ref}\nu_i W_i \tag{4.61}$$

The combustion heat is calculated by summing:

$$Q = \sum_{i=1}^{n} h_i \nu_i' W_i \tag{4.62}$$

$$\Rightarrow Q_{ref} = \sum_{i=1}^{n} h_{i,ref}\nu_i' W_i, \tag{4.63}$$

since this value does not vary significantly with temperature thus reference values are taken.

Assuming $T_{ref} = T_u$, $Q = Q_{ref}$, $\nu_i = -\nu_i'$, $c_{p,u} = 0$ and $c_{p,b}$ approximately constant and using equations (4.56) and (4.61), for lean combustion ($Y_{F,b} = 0$), that is, for $Z < Z_{st}$, we have:

$$\frac{Y_{F,u}Q_{ref}}{\nu_F W_F} = \int_{T_u}^{T_b} c_p dT \tag{4.64}$$

$$\Rightarrow T_b - T_u = \frac{Q_{ref}}{c_p \nu_F W_F} Y_{F,u}. \tag{4.65}$$

For a rich mixture, we adopt the same procedure as from equation (4.59) replacing the fuel with the oxidant. Then, for $Z \geq Z_{st}$ we have:

$$\Rightarrow T_b - T_u = \frac{Q_{ref}}{c_p \nu_{O_2} W_{O_2}} Y_{O_2,u}. \tag{4.66}$$

Therefore, the Burke-Schumann solution for temperature is defined by:

$$T_b(Z) = T_u(Z) + \frac{Q_{ref}}{c_p \nu_F W_F} Y_{F,1} Z, \text{ if } Z < Z_{st}; \tag{4.67}$$

$$T_b(Z) = T_u(Z) + \frac{Q_{ref}}{c_p \nu_{O_2} W_{O_2}} Y_{O_2,2}(1 - Z), \text{ if } Z \geq Z_{st}. \tag{4.68}$$

4.1.2 Mixture Fraction with Multi-parameters

In larger mechanisms, it is not possible to obtain information about the concentrations of compounds in the intermediate reactions of the combustion process using the previous approach. Therefore, the mixture fraction is normally decomposed into constitutive terms that represent the mass fractions of the elements contained in the fuel stream [36]:

$$Z = Z_1 + Z_2 + \cdots + Z_n, \tag{4.69}$$

where n is the number of components.

As an example, we consider a global two-step mechanism for the combustion of MD:

$$\begin{cases} C_{11}H_{22}O_2 + 10CO_2 & \rightleftharpoons 11CO + 11H_2O \\ CO + 0.5O_2 & \rightleftharpoons CO_2; \end{cases} \tag{4.70}$$

the chemical species that contain carbon are MD, CO and CO_2. According to the mass conservation law:

$$\frac{dY_{MD}}{\nu_{MD}W_{MD}} + \frac{dY_{CO}}{\nu_{CO}W_{CO}} + \frac{dY_{CO}}{\nu_{CO_2}W_{CO_2}} = 0. \tag{4.71}$$

Integrating the equation from a time before burning to some moment after combustion and taking $Y_{CO,u} = Y_{CO_2,u} = 0$, we have:

$$\frac{1}{W_{MD}}\big(Y_{MD} - Y_{MD,1}Z\big) + \frac{1}{\nu_{CO}W_{CO}}Y_{CO} + \frac{1}{\nu_{CO_2}W_{CO_2}}Y_{CO_2} = 0. \tag{4.72}$$

Which means:

$$Z = \frac{W_{MD}}{Y_{MD,1}}\left[\frac{Y_{MD}}{W_{MD}} + \frac{Y_{CO}}{\nu_{CO}W_{CO}} + \frac{Y_{CO_2}}{\nu_{CO_2}W_{CO_2}}\right]. \tag{4.73}$$

For convenience, we write the mass fractions of each carbon-containing species as:

$$Z_1 = \frac{Y_{MD}}{Y_{MD,1}}, \tag{4.74}$$

$$Z_2 = \frac{W_{MD}}{\nu_{CO} Y_{MD,1} W_{CO}} Y_{CO}, \tag{4.75}$$

$$Z_3 = \frac{W_{MD}}{\nu_{CO_2} Y_{MD,1} W_{CO_2}} Y_{CO_2}. \tag{4.76}$$

This way, we can determine the mass fraction of each component of the mixture fraction even for larger mechanisms.

4.2 Reactive Flow Equations

The vector equation for the conservation of mass is defined by [5]:

$$\frac{\partial \rho}{\partial t} + \nabla \cdot (\rho \mathbf{u}) = 0, \tag{4.77}$$

where ρ is the specific density, t is time, ∇ is the divergent operator, and $\mathbf{u}$ is the velocity vector. Considering the three-dimensional Cartesian system, we can write the **mass conservation equation** as:

$$\frac{\partial \rho}{\partial t} + \frac{\partial}{\partial x_j}(\rho u_j) = 0, \quad j = 1, 2, 3. \tag{4.78}$$

The **momentum conservation equation** describes the velocity field and it is defined by:

$$\frac{\partial}{\partial t}(\rho \mathbf{u}) + \nabla \cdot (\rho \mathbf{u}\mathbf{u}) = -\nabla p + \nabla \cdot J + \rho \mathbf{g}, \tag{4.79}$$

where p is the pressure, J is the tensor of viscous stresses which represents the molecular transport due to viscosity, and g is the vector of field forces.

The expression $\mathbf{uu}$ indicates the outer product of the velocity vectors $\mathbf{u}$, that is, $\mathbf{uu}$ is a matrix. In the index notation we write $(\mathbf{uu})_{ij} = u_i u_j$. We also express the momentum conservation equation by:

$$\frac{\partial}{\partial t}(\rho u_i) + \frac{\partial}{\partial x_j}(\rho u_i u_j) = -\frac{\partial p}{\partial x_i} + \frac{\partial}{\partial x_j} J_{ij} + \rho g_i, \tag{4.80}$$

where J_{ij} is:

$$J_{ij} = \mu\left[2S_{ij} - \frac{2}{3}\delta_{ij}\frac{\partial u_k}{\partial x_k}\right], \tag{4.81}$$

where μ is the dynamic viscosity and δ_{ij} is the Kronecker Delta defined as [5]:

$$\delta_{ij} = \begin{cases} 1, \text{ se } i = j; \\ 0, \text{ se } i \neq j. \end{cases} \tag{4.82}$$

We express the deformation tensor S by:

$$S = \frac{1}{2}\left(\frac{\partial u_i}{\partial x_j} + \frac{\partial u_j}{\partial x_i}\right). \tag{4.83}$$

The energy equation can be expressed in terms of temperature. Assuming the same heat capacities for all species and discarding radiation and field forces, we define the **energy equation** in vector notation as:

$$\frac{\partial}{\partial t}(\rho T) + \nabla(\rho \mathbf{u} T) = \nabla \cdot \left(\frac{\lambda}{c_p}\nabla T\right) + \dot{\omega}_T, \tag{4.84}$$

and using index notation we have:

$$\frac{\partial}{\partial t}(\rho T) + \frac{\partial}{\partial x_j}(\rho u_j T) = \frac{\partial}{\partial x_j}\left(\frac{\lambda}{c_p}\frac{\partial T}{\partial x_j}\right) + \dot{w}_T, \tag{4.85}$$

where λ is the thermal conductivity, c_p is the specific heat at constant pressure and $\dot{w}_T$ is the energy source term, that is, it is the heat generation rate, defined by:

$$\dot{w}_T = \frac{1}{c_p}\sum_{k=1}^{r}\dot{\omega}_k Q_k, \tag{4.86}$$

where $\dot{\omega}_k$ is the chemical source term and Q_k is the combustion heat of the reaction k calculated by the equation (4.62).

Although the pressure effects are small, they are locally important. In addition, pressure gradients also correct velocity fields. The **pressure equation** is here defined by [77]:

$$\nabla^2 p = \Delta t\left(\frac{\partial \rho}{\partial t} + \frac{\partial}{\partial x_j}(\rho \mathbf{u})\right); \tag{4.87}$$

where Δt is a time step.

The density equation was approximated considering that it depends on atmospheric pressure and temperature. Now we take the **density equation** as [26]:

$$\rho = p_0 \left[1 + \frac{\sigma}{T(1-\sigma)} \right]^{-1}, \tag{4.88}$$

where p_0 is the atmospheric pressure and $0.1 < \sigma < 0.8$ is the relaxation coefficient.

The mass fraction equation of chemical species can be expressed vectorially by [74, 103]:

$$\frac{\partial}{\partial t}(\rho Y_i) + \nabla(\rho \mathbf{u} Y_i) = \nabla(\rho G_i \nabla \mathrm{Y}_i) \pm \dot{\omega}_i, \qquad i = 1, 2, 3, \ldots, n; \tag{4.89}$$

where Y_i is the mass fraction of the species i, G_i is the mass diffusivity of the species i and $\dot{\omega}_i$ is the chemical source term, defined by the reaction rate of the species i. The chemical reaction rate $\dot{\omega}_i$, which is the mass of the species i consumed or generated per unit of volume and unit of time, is the sum of all reaction rates of the mechanism:

$$\dot{\omega}_i = W_i \sum_{k=1}^{r} \nu_{ik} \omega_k, \tag{4.90}$$

where W_i is the molecular weight of the species i, r is the number of chemical reactions in the mechanism and $\nu_{ik} = \nu_{ik}^{''} - \nu_{ik}^{'}$ is the stoichiometric coefficient of the species i in the reaction k. The rate of the reaction k in the r-containing chemical reactions mechanism is given by:

$$\omega_k = k_{fk} \prod_{j=1}^{n} \left(\frac{\rho Y_j}{W_j} \right)^{\nu_{jk}^{'}} - k_{bk} \prod_{j=1}^{n} \left(\frac{\rho Y_j}{W_j} \right)^{\nu_{jk}^{''}}, \tag{4.91}$$

where k_{fk} and k_{bk} are the specific velocities of the reaction k in the forward and reverse directions, respectively.

The mixture fraction Z can be calculated by a conservative equation, which means no source terms, since it represents the chemical elements that make up the fuel jet and the elements are preserved during combustion.

Replacing equations (4.74), (4.75) and (4.76) in the conservation equation of the species mass fraction (4.89) and taking $G_i = G$, which means that all diffusivities are equal, we obtain the mixture fraction equation system:

$$\frac{\partial(\rho Z_1)}{\partial t} + \frac{\partial(\rho u_j Z_1)}{\partial x_j} = \frac{\partial}{\partial x_j}\left(\rho G \frac{\partial Z_1}{\partial x_j}\right) - \dot{\omega}_{CO,I}, \tag{4.92}$$

$$\frac{\partial(\rho Z_2)}{\partial t} + \frac{\partial(\rho u_j Z_2)}{\partial x_j} = \frac{\partial}{\partial x_j}\left(\rho G \frac{\partial Z_2}{\partial x_j}\right) + \dot{\omega}_{CO,I} - \dot{\omega}_{CO,II}, \tag{4.93}$$

$$\frac{\partial(\rho Z_3)}{\partial t} + \frac{\partial(\rho u_j Z_3)}{\partial x_j} = \frac{\partial}{\partial x_j}\left(\rho G \frac{\partial Z_3}{\partial x_j}\right) + \dot{\omega}_{CO,II}. \tag{4.94}$$

When we add the system of equations, we obtain the **mixture fraction equation** written as [103]:

$$\frac{\partial(\rho Z)}{\partial t} + \frac{\partial(\rho u_j Z)}{\partial x_j} = \frac{\partial}{\partial x_j}\left(\rho G \frac{\partial Z}{\partial x_j}\right). \tag{4.95}$$

4.3 Turbulent Flow

In both nature and engineering applications, the flow tends to be turbulent. Turbulence can be defined by the chaotic behavior of the trajectory of the fluid particle forming eddies and vortices [17]. This way the movement variables exhibit spatial and temporal fluctuations [44]. In combustion, the turbulent effect is advantageous because it makes the mixture process faster and also increases the energy dissipation gradient. Turbulent diffusion flames are used in diesel engines, boilers, industrial furnaces and turbojet engine with afterburner.

The reactive turbulent flow can be modeled by the Navier-Stokes equations added to the chemical species conservation equations. Due to fluctuations, the direct solution of the Navier-Stokes equations is impractical. Computational fluid dynamics applies numerical procedures for simulating turbulent reactive flows, such as DNS, LES and RANS.

The Direct Numerical Simulation (DNS) technique solves the reactive flow equations directly without modeling simplifications. This way, a wide set of temporal and spatial scales are solved [117], which is computationally highly expensive.

On the other hand, the Reynolds Averaged Navier-Stokes (RANS) technique requires small computational resources when compared to the other approaches. In this technique, the flow variables are decomposed into two terms of average values and fluctuating values. In this process, an additional term to the total shear stress appears, named Reynolds tensor, which must be modeled and then the equations solved [2].

The decomposition of variables is defined by $\Phi = \overline{\Phi} + \Phi'$, where $\overline{\Phi}$ represents the average value and Φ' is the floating value, with $\overline{\Phi'} = 0$. The average value is calculated over time as

$$\overline{\Phi} = \lim_{\Delta t \to +\infty} \left(\frac{1}{\Delta t} \int_{t_0}^{t_0+\Delta t} \Phi(t) dt \right). \tag{4.96}$$

For Φ and Ψ, variables of interest, the Reynolds-averaging presents the properties:

i) $\overline{\overline{\Phi}} = \overline{\Phi}$;

ii) $\overline{\Phi \cdot \overline{\Psi}} = \overline{(\overline{\Phi} + \Phi') \cdot \overline{\Psi}} = \overline{\Phi} \cdot \overline{\Psi}$;

iii) $\overline{\Phi' \cdot \overline{\Psi}} = 0$;

iv) $\overline{\Phi + \Psi} = \overline{(\overline{\Phi} + \Phi') + (\overline{\Psi} + \Psi')} = \overline{\Phi} + \overline{\Psi}$;

v) $\dfrac{\overline{\partial \Phi}}{\partial x} = \dfrac{\partial (\overline{\overline{\Phi} + \phi'})}{\partial x} = \dfrac{\partial \overline{\Phi}}{\partial x}$;

vi) $\overline{\int \Phi dx} = \int \overline{(\overline{\Phi} + \Phi)'} dx = \int \overline{\Phi} dx$.

The Large Eddy Simulation (LES) technique resembles RANS in decomposing the variable into medium and fluctuating terms. However, the LES approach also applies a spatial filter that separates the length scales into large and small scales [24]. On large scales, a large part of the kinetic energy of the system is concentrated, and therefore, the average values will be computed numerically. At small scales there is a small portion of energy, thus, fluctuating values can be modelled. The LES technique is a compromise between the DNS and the RANS technique, both in computational costs and in the accuracy of the results obtained.

In addition to the Reynolds-averaging, it is common to also use the Favre-averaging, whose averaged values are weighted by the specific density. Favre-averaging is indicated in turbulent combustion due to density fluctuations. In Favre-averaging, we consider $\Phi = \tilde{\Phi} + \Phi''$, where $\tilde{\Phi}$ represents the averaged value and Φ'' is the floating value, with $\overline{\rho\Phi''} = 0$. The average value of Favre is calculated by:

$$\tilde{\Phi} = \frac{\overline{\rho\Phi}}{\overline{\rho}} = \lim_{\Delta t \to +\infty} \left(\frac{\int_t^{t+\Delta t} \rho\Phi(t)dt}{\int_t^{t+\Delta t} \rho dt} \right). \tag{4.97}$$

The properties of Favre-averaging are $\overline{\rho\Phi} = \overline{\rho}\tilde{\Phi}$ and $\overline{\rho\tilde{\Phi}} = \overline{\rho}\tilde{\Phi}$.

Applying the Favre-averaging to the reactive turbulent flow equations we obtain the turbulent flow equations:

1. Continuity Equation:

$$\frac{\partial\overline{\rho}}{\partial t} + \frac{\partial(\overline{\rho}\tilde{u})}{\partial x} + \frac{\partial(\overline{\rho}\tilde{v})}{\partial y} + \frac{\partial(\overline{\rho}\tilde{w})}{\partial z} = 0. \tag{4.98}$$

2. Momentum Conservation Equations:

$$\begin{aligned}\overline{\rho}\left(\frac{\partial\tilde{u}}{\partial t} + \tilde{u}\frac{\partial\tilde{u}}{\partial x} + \tilde{v}\frac{\partial\tilde{u}}{\partial y} + \tilde{w}\frac{\partial\tilde{u}}{\partial z}\right) = &-\frac{\partial\overline{p}}{\partial x} + \mu\left(\frac{\partial^2\tilde{u}}{\partial x^2} + \frac{\partial^2\tilde{u}}{\partial y^2} + \frac{\partial^2\tilde{u}}{\partial z^2}\right) \\ &- \frac{\partial}{\partial x}\left(\overline{\rho}\widetilde{u''u''} + \overline{\rho}\widetilde{u''v''} + \overline{\rho}\widetilde{u''w''}\right);\end{aligned} \tag{4.99}$$

$$\overline{\rho}\left(\frac{\partial\tilde{v}}{\partial t}+\tilde{u}\frac{\partial\tilde{v}}{\partial x}+\tilde{v}\frac{\partial\tilde{v}}{\partial y}+\tilde{w}\frac{\partial\tilde{v}}{\partial z}\right)=-\frac{\partial\overline{p}}{\partial y}+\mu\left(\frac{\partial^2\tilde{v}}{\partial x^2}+\frac{\partial^2\tilde{v}}{\partial y^2}+\frac{\partial^2\tilde{v}}{\partial z^2}\right)$$
$$-\frac{\partial}{\partial y}\left(\overline{\rho}\widetilde{v''u''}+\overline{\rho}\widetilde{v''v''}+\overline{\rho}\widetilde{v''w''}\right); \qquad (4.100)$$

$$\overline{\rho}\left(\frac{\partial\tilde{w}}{\partial t}+\tilde{u}\frac{\partial\tilde{w}}{\partial x}+\tilde{v}\frac{\partial\tilde{w}}{\partial y}+\tilde{w}\frac{\partial\tilde{w}}{\partial z}\right)=-\frac{\partial\overline{p}}{\partial z}+\mu\left(\frac{\partial^2\tilde{w}}{\partial x^2}+\frac{\partial^2\tilde{w}}{\partial y^2}+\frac{\partial^2\tilde{w}}{\partial z^2}\right)$$
$$-\frac{\partial}{\partial z}\left(\overline{\rho}\widetilde{w''u''}+\overline{\rho}\widetilde{w''v''}+\overline{\rho}\widetilde{w''w''}\right). \qquad (4.101)$$

3. Chemical Species Mass Fraction Equation:

$$\overline{\rho}\left(\frac{\partial\tilde{Y}_i}{\partial t}+\tilde{u}\frac{\partial\tilde{Y}_i}{\partial x}+\tilde{v}\frac{\partial\tilde{Y}_i}{\partial y}+\tilde{w}\frac{\partial\tilde{Y}_i}{\partial z}\right)=\overline{\rho}\overline{D}\left(\frac{\partial^2\tilde{Y}_i}{\partial x^2}+\frac{\partial^2\tilde{Y}_i}{\partial y^2}+\frac{\partial^2\tilde{Y}_i}{\partial z^2}\right)\pm\widetilde{\dot{\omega}}_i$$
$$-\frac{\partial}{\partial x}\left(\overline{\rho}\widetilde{u''Y_i''}\right)-\frac{\partial}{\partial y}\left(\overline{\rho}\widetilde{v''Y_i''}\right)-\frac{\partial}{\partial z}\left(\overline{\rho}\widetilde{w''Y_i''}\right). \qquad (4.102)$$

4. Mixture Fraction Equation:

$$\overline{\rho}\left(\frac{\partial\tilde{Z}}{\partial t}+\tilde{u}\frac{\partial\tilde{Z}}{\partial x}+\tilde{v}\frac{\partial\tilde{Z}}{\partial y}+\tilde{w}\frac{\partial\tilde{Z}}{\partial z}\right)=\overline{\rho}\overline{D}\left(\frac{\partial^2\tilde{Z}}{\partial x^2}+\frac{\partial^2\tilde{Z}}{\partial y^2}+\frac{\partial^2\tilde{Z}}{\partial z^2}\right)$$
$$-\frac{\partial}{\partial x}\left(\overline{\rho}\widetilde{u''Z''}\right)-\frac{\partial}{\partial y}\left(\overline{\rho}\widetilde{v''Z''}\right)-\frac{\partial}{\partial z}\left(\overline{\rho}\widetilde{w''Z''}\right). \qquad (4.103)$$

5. Energy Equation:

$$\overline{\rho}\left(\frac{\partial\tilde{T}}{\partial t}+\tilde{u}\frac{\partial\tilde{T}}{\partial x}+\tilde{v}\frac{\partial\tilde{T}}{\partial y}+\tilde{w}\frac{\partial\tilde{T}}{\partial z}\right)=\frac{\overline{\lambda}}{c_p}\left(\frac{\partial^2\tilde{T}}{\partial x^2}+\frac{\partial^2\tilde{T}}{\partial y^2}+\frac{\partial^2\tilde{T}}{\partial z^2}\right)+\frac{1}{c_p}\widetilde{\dot{\omega}_T}$$
$$-\frac{\partial}{\partial x}\left(\overline{\rho}\widetilde{u''T''}\right)-\frac{\partial}{\partial y}\left(\overline{\rho}\widetilde{v''T''}\right)-\frac{\partial}{\partial z}\left(\overline{\rho}\widetilde{w''T''}\right). \qquad (4.104)$$

6. Pressure Equation:

$$\nabla^2\overline{p}=\Delta t\left[\frac{\partial\overline{\rho}}{\partial t}+\frac{\partial(\overline{\rho}\tilde{u})}{\partial x}+\frac{\partial(\overline{\rho}\tilde{v})}{\partial y}+\frac{\partial(\overline{\rho}\tilde{w})}{\partial z}\right]. \qquad (4.105)$$

7. Density Equation:

$$\overline{\rho}=\overline{p}_0\left[1+\frac{\sigma}{\widetilde{T}(1-\sigma)}\right]^{-1}. \qquad (4.106)$$

The term $\overline{\rho}\widetilde{u_i''u_j''}$ is named Reynolds tensor and it represents the stress exerted by turbulent fluctuations in the fluid. The terms $\overline{\rho}\widetilde{u_j''Z''}$ and $\overline{\rho}\widetilde{u_j''T''}$ correspond to mass transport and the temperature rate, respectively, due to turbulent fluctuations in the flow.

These terms must be modeled. For the Reynolds tensor, Boussinesq (1897) [15] developed a model assuming that the tensor is approximated by the velocity gradient written as

$$-\overline{\rho}\widetilde{u''v''} = \overline{\rho}\mu_T\frac{\partial\tilde{u}}{\partial y}, \tag{4.107}$$

where μ_T is a proportionality constant named turbulent viscosity.

4.3.1 Turbulent Viscosity

Turbulent viscosity is a characteristic artificial flow parameter. Turbulent viscosity was considered constant by Boussinesq, however, other authors consider it spatially variable. Next, we present some widely used models for modeling turbulent viscosity.

Agrawal-Prasad Model

Agrawal & Prasad (2003) [1] suggested analytical solutions for turbulent viscosity in planar and axisymmetric turbulent jets. For the axisymmetric model, we consider the continuity and momentum equations, three-dimensional, in the preferred x-direction, with y and z varying with the radius $r = \sqrt{y^2 + z^2}$. The velocity profile on the centerline of the jet, U_c, behaves similarly to the curve $x^{-1/2}$ and the characteristic length is taken as $b \approx x$. The analytical expression for turbulent viscosity is given by:

$$\mu_T = U_c b\frac{\sqrt{\pi}}{8}c\frac{erf(\xi)}{\xi};\quad \xi = \frac{r}{cx}, \tag{4.108}$$

where c is a parameter of the solution and $c \simeq 0.107$ is usually assumed.

Smagorinsky Model

The most classic model used in LES is the Smagorinsky model (1963) [94]. The equation proposed by Smagorinsky derives from the hypothesis of a balance between the production and isotropic dissipation of turbulent kinetic energy, and it is defined as:

$$\mu_T = (C_S\Delta)^2|\overline{S}|_F; \tag{4.109}$$

where $0 < C_S < 1$ is the Smagorinsky coefficient, $\Delta = (\Delta x \Delta y \Delta z)^{\frac{1}{3}}$ is the size of the filter used in the mesh, and $|\overline{S}|_F$ is the Frobenius norm for the strain tensor S_{ij}. The Frobenius norm [49] is defined by $|\overline{S}|_F = \sqrt{\sum_{j=1}^{3}\sum_{i=1}^{3}|S_{ij}|^2}$, that is,

$$|\overline{S}|_F = \left\{ \frac{1}{2}\left[\left(\frac{\partial u}{\partial y}\right)^2 + \left(\frac{\partial u}{\partial z}\right)^2 + \left(\frac{\partial v}{\partial x}\right)^2 + \left(\frac{\partial v}{\partial z}\right)^2 + \left(\frac{\partial w}{\partial x}\right)^2 + \left(\frac{\partial w}{\partial y}\right)^2 \right] + \right.$$
$$\left. + \left(\frac{\partial u}{\partial x}\right)^2 + \left(\frac{\partial v}{\partial y}\right)^2 + \left(\frac{\partial w}{\partial z}\right)^2 + \frac{\partial u}{\partial y}\frac{\partial v}{\partial x} + \frac{\partial u}{\partial z}\frac{\partial w}{\partial x} + \frac{\partial v}{\partial z}\frac{\partial w}{\partial y} \right\}^{\frac{1}{2}}. \tag{4.110}$$

In this work, at first we use the Agrawal-Prasad model for turbulent viscosity and then we test the Smagorinsky model. We noticed that the differences produced in the velocity field and in the mixture fraction were small, in the order of 10^{-2}; therefore we continue to use the Agrawal-Prasad model.

4.4 Dimensionless Equations

In CFD, there is usually a high number of variables and parameters, which have different magnitudes, units and can be related through implicit relations. Dimensional analysis exposes these combinations of parameters and variables to reduce computational memory, while maintaining the completeness and homogeneity of the equations.

The idea of dimensional analysis is to divide each term of the equation by a set of variables and parameters with similar magnitude of the term. This procedure causes the scales of all terms to be unified.

To obtain the dimensionless equations of the reactive turbulent flow, we made the following substitutions:

i) Spatial and temporal components:

$$x^* = \frac{x}{L},\ y^* = \frac{y}{L},\ z^* = \frac{z}{L},\ t^* = \frac{V_0 t}{L}; \tag{4.111}$$

ii) Velocity components:

$$\widetilde{u}^* = \frac{\widetilde{u}}{V_0},\ \widetilde{v}^* = \frac{\widetilde{v}}{V_0},\ \widetilde{w}^* = \frac{\widetilde{w}}{V_0}; \tag{4.112}$$

iii) Density and pressure equations:

$$\overline{\rho}^* = \frac{\overline{\rho}}{\overline{\rho}_{st}},\ \overline{p}^* = \frac{\overline{p} - \overline{p}_0}{\overline{\rho} V_0^2}; \tag{4.113}$$

iv) Mass fraction equations:

$$\widetilde{Y}_F^* = \frac{\widetilde{Y}_F}{Y_{F,u}},\ \widetilde{Y}_{O_2}^* = \frac{\widetilde{Y}_{O_2}}{Y_{O_2,u}},\ \widetilde{Y}_P^* = \left(\nu \frac{Y_{F,u}}{Y_{O_2,u}} + 1\right) \frac{\nu_F W_F}{\nu_P W_P} \frac{\widetilde{Y}_P}{Y_{F,u}}; \tag{4.114}$$

v) Temperature equation and parameters:

$$\widetilde{T}^* = \frac{\widetilde{T} - \widetilde{T}_u}{\widetilde{T}_b - \widetilde{T}_u},\ \widetilde{T}_b = \widetilde{T}_u + \frac{Q_{ref} Y_{F,u} \widetilde{Y}_{O_2}}{c_p \nu_F W_F (\nu Y_{F,u} + \widetilde{Y}_{O_2})}; \tag{4.115}$$

vi) Dimensionless numbers and parameters:

$$Re = \frac{\overline{\rho} D V_0}{\mu},\ Sc = \frac{\mu}{\overline{\rho}\overline{D}},\ Pr = \frac{c_p \mu}{\overline{\lambda}}, Ze = \varsigma\zeta, \tag{4.116}$$

$$\varsigma = \frac{\widetilde{T}_b - \widetilde{T_u}}{\widetilde{T}_b},\ \zeta = \frac{E}{R\widetilde{T}_b}; \tag{4.117}$$

where V_0 index refers to a reference velocity, L is a reference length, Re is the Reynolds number, Sc is the Schmidt number, Pr is the Prandtl number and Ze is the Zel'dovich number.

Therefore, we write the system of reactive turbulent flow equations as:

$$\begin{cases} \dfrac{\partial(\overline{\rho}\widetilde{u}_i)}{\partial t} + \dfrac{\partial(\overline{\rho}\widetilde{u}_i\widetilde{u}_j)}{\partial x_j} = -\dfrac{\partial \overline{p}}{\partial x_j} + \dfrac{\partial}{\partial x_j}\left(\dfrac{\mu_T}{Re}\dfrac{\partial \widetilde{u}_i}{\partial x_j}\right); \\ \dfrac{\partial(\overline{\rho}\widetilde{Y}_k)}{\partial t} + \dfrac{\partial(\overline{\rho}\widetilde{u}_j\widetilde{Y}_k)}{\partial x_j} = \dfrac{\partial}{\partial x_j}\left(\dfrac{\mu_T}{Re\ Sc}\dfrac{\partial \widetilde{Y}_k}{\partial x_j}\right) \pm \overline{\dot{\omega}_k}; \qquad k = 1, \ldots, n; \\ \dfrac{\partial(\overline{\rho}\widetilde{u}_j\widetilde{Z})}{\partial t} + \dfrac{\partial(\overline{\rho}\widetilde{Z})}{\partial x_j} = \dfrac{\partial}{\partial x_j}\left(\dfrac{\mu_T}{Re\ Sc}\dfrac{\partial \widetilde{Z}}{\partial x_j}\right); \\ \dfrac{\partial(\overline{\rho}\widetilde{T})}{\partial t} + \dfrac{\partial(\overline{\rho}\widetilde{u}_j\widetilde{T})}{\partial x_j} = \dfrac{\partial}{\partial x_j}\left(\dfrac{\overline{\rho}\ \mu_T}{Pr}\dfrac{\partial \widetilde{T}}{\partial x_j}\right) + \overline{\dot{\omega}_T}; \\ \nabla^2\overline{p} = \Delta t\left[\dfrac{\partial \overline{\rho}}{\partial t} + \dfrac{\partial(\overline{\rho}\widetilde{u}_j)}{\partial x_j}\right]; \\ \overline{\rho} = \overline{p}_0\left[1 + \frac{\sigma}{\widetilde{T}(1-\sigma)}\right]^{-1}. \end{cases} \tag{4.118}$$

5 PROBLEM SETUP

In this chapter we describe the configuration and characteristics of the proposed problem. We present the type of flame, the burner dimensions, the computational mesh, the initial conditions and the boundary conditions for the system variables.

5.1 Turbulent Jet Diffusion Flame

During combustion there are regions of small thickness where the temperature gradients are higher than in the other regions, which makes the combustion non-homogeneous. This narrow extension emits light and it is called a flame.

Combustion can be premixed or non-premixed. In the premixed flame, fuel and oxidant are mixed at the molecular level in an antechamber before burning. During burning, we noticed the formation of a flame front propagating with a characteristic velocity until the total consumption of the fuel-oxidant mixture [74]. In this configuration, flames are smaller, uniform and locally intense. Internal combustion engines with spark plug, gas turbines and Bunsen burners are examples of applications for the premixed flame.

The nonpremixed flame is fed by two distinct jets containing fuel and oxidant separately. Fuel and oxidant are released into the same environment at a certain velocity and they mix at the molecular level by convection and diffusion during the ignition process [74]. As diffusion is the main transport phenomenon of this process, it is well accepted to call the nonpremixed flame a diffusive flame.

The geometrical locus where the fuel and the oxidant are in stoichiometric proportion is named stoichiometric region and at this interface the largest

temperature gradients and reaction rates of the chemical species occur. Figure (5.1) shows a diffusion flame sketch.

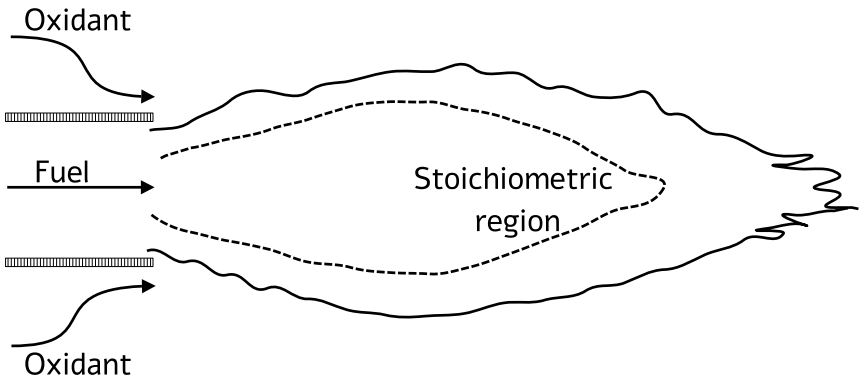

Figure 5.1: Diffusion flame sketch.

Diffusion flame can be coflow, in which the flame is formed by two distinct flows of fuel and oxidant injected in the same direction; or counterflow, in which the flame is formed between two distinct potential flows of oxidant and fuel with opposite directions [102].

In this work we use the coflow flame which has a geometry similar to a free jet. A free jet is characterized as a non-zero velocity pressurized fluid stream launched through an inlet pipe in an infinite fluid-at-rest environment.

The flow can be divided in three regions as shown in Fig. (5.2). In the field region near the inlet there is the potential core of the jet where the viscous and frictional effects are not yet effective and the fluid leaving the pipe drags the external fluid and spreads radially, slowing down as it moves away from the inlet. The second region is the transition zone, where the jet velocity decreases and the pressure gradient increases. The third region is the far field zone, in which the flow is fully developed, the effects of the initial conditions do not affect the fluid and the radial velocity distributions are identical [97].

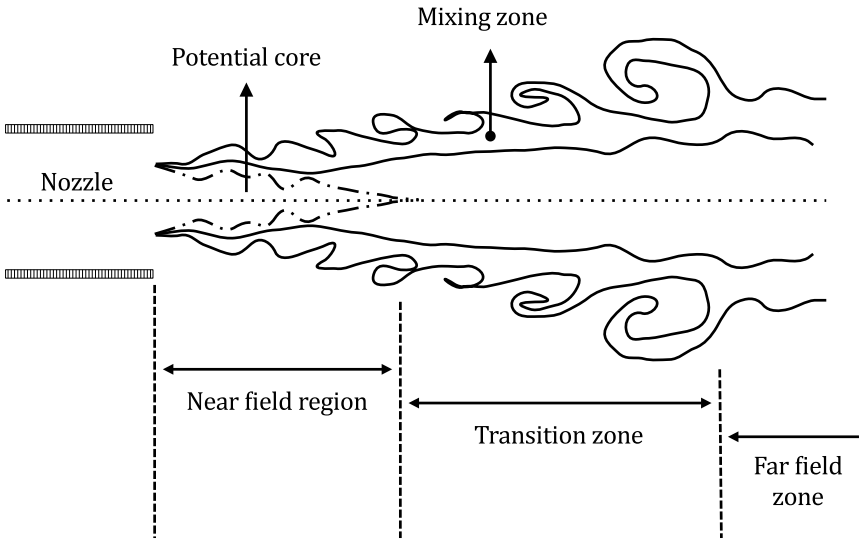

Figure 5.2: Free jet sketch.

Experimental and numerical simulation studies on free jet have been carried out extensively in recent years, since there are several applications of this type of flow, such as in fuel injectors and industrial combustion processes [100].

Fuel changes from the liquid phase to the gas phase as the system temperature increases, which causes the fuel droplets to be consumed from the outside to the inside [31]. In this work, we assume that the fuel is released into the pre-vaporized burner. The fuel vaporization before the burning process accelerates the fuel-oxidant mixture at the molecular level, making it more efficient, in addition to contributing to a more complete burning, reducing the emission of pollutants.

As a reference, we use the Sandia Flame D, proposed by Sandia National Laboratories [8], in which the fuel jet is surrounded by a pilot. The pilot releases a flame at a lower velocity, compared to the fuel jet, and its function is to stabilize the main jet. This type of burner was developed and studied by Masri et al (1996) [59] at The University of Sydney.

Figure (5.3) illustrates the burner with lengths $L = 11$, $h = 1$, w $= 1$, $d \approx 0.11163$, $D \approx 0.2844$, which have been adapted from [8].

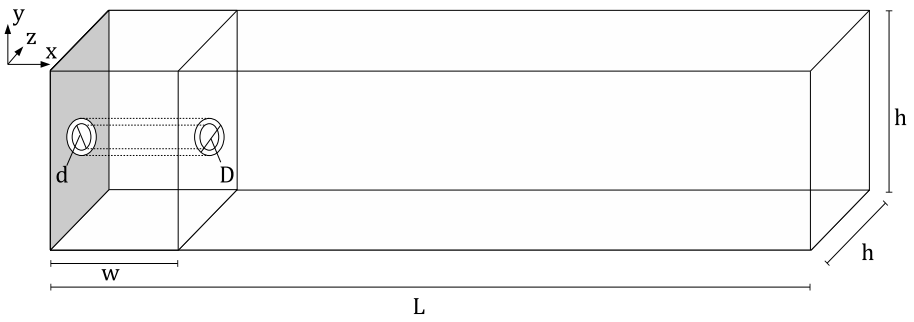

Figure 5.3: Burner sketch.

5.2 Computational Domain and Mesh

The mesh is structured, rectangular and non-uniform. We refine the mesh in the regions with the highest gradients of the variables of interest. The use of a mesh suitable for the proposed problem has great relevance in obtaining the solution [57, 25]. Among the advantages of a structured mesh, we highlight the construction of a simple function that connects the dots and of easy computational implementation.

The two-dimensional mesh used contains 251×51 nodes and the three-dimensional mesh, $251 \times 51 \times 51$ nodes. A longitudinal section of the mesh, showing the interval [0.5,5], is illustrated in Fig. (5.4).

5.3 Initial Conditions and Boundary Conditions

Obtaining the numerical solution of the system of equations requires the application of initial and boundary conditions. The initial conditions refer to

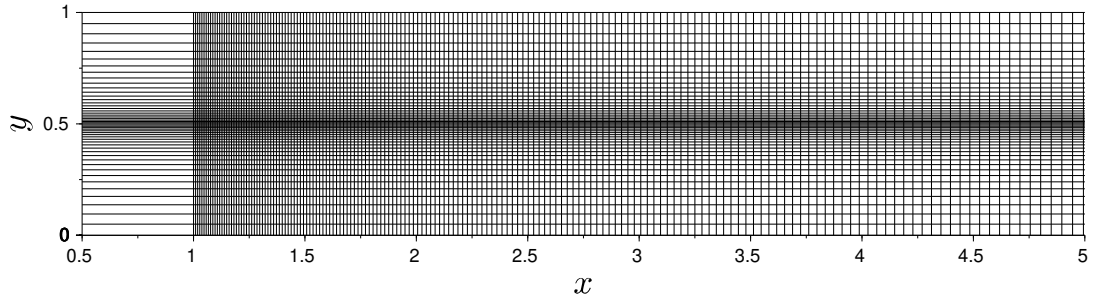

Figure 5.4: Two-dimensional mesh sketch in the x and y-directions.

the start of combustion, at time $t_0 = 0$, and are given by the equations (5.1) to (5.10):

$$\widetilde{u}(x,y,z,t_0) = \begin{cases} \widetilde{u}_\infty\big[1-(\frac{r}{d})^2\big], \text{ if } 0 \le x \le l, \text{ and } r \le d; \\ 0.23\widetilde{u}_\infty, \text{ if } 0 \le x \le l, \text{ and } d \le r \le D; \\ 0.02\widetilde{u}_\infty, \text{ otherwise;} \end{cases} \tag{5.1}$$

$$\widetilde{v}(x,y,z,t_0) = 0; \tag{5.2}$$

$$\widetilde{w}(x,y,z,t_0) = 0; \tag{5.3}$$

$$\widetilde{Z}(x,y,z,t_0) = \begin{cases} 1, \text{ if } 0 \le x \le l, \text{ and } r \le d; \\ 0, \text{ otherwise;} \end{cases} \tag{5.4}$$

$$\widetilde{Y_F}(x,y,z,t_0) = \begin{cases} Y_{F,u}, \text{ if } 0 \le x \le l, \text{ and } r \le d; \\ 0, \text{ otherwise;} \end{cases} \tag{5.5}$$

$$\widetilde{Y_{O_2}}(x,y,z,t_0) = \begin{cases} 0, \text{ if } 0 \le x \le l, \text{ and } r \le d; \\ Y_{O_2,u}, \text{ otherwise;} \end{cases} \tag{5.6}$$

$$\widetilde{Y_P}(x,y,z,t_0) = 0; \tag{5.7}$$

$$\widetilde{T}(x,y,z,t_0) = T_\infty; \tag{5.8}$$

$$\overline{p}(x,y,z,t_0) = 1; \tag{5.9}$$

$$\overline{\rho}(x,y,z,t_0) = \rho_\infty; \tag{5.10}$$

where Y_P represents the mass fraction of the species P involved in combustion.

The values used in Refs. [8, 9] were normalized due to the dimensional analysis done in this work, as described in table (5.3). Although some variables are presented in their dimensional values, such as temperature.

Table 5.1: Parameter conversion.

	Sandia Flame D Conditions	Normalized Conditions
Main jet velocity	$u_F = 49.6\ m/s$	$u_\infty = 1$
Pilot jet Velocity	$u_p = 11.4\ m/s$	$u_p = 0.23$
Coflow jet velocity	$u_c = 0.9\ m/s$	$u_c = 0.02$
Temperature	$T_\infty = 300K$	$T_\infty = 1$
Ambient Pressure	$p_\infty = 1\ atm$	$p_\infty = 1$
Density	-	$\rho_\infty = 1$

Dirichlet boundary conditions, when the value of the variable is known, or Neumann boundary conditions, when the value of the flow is known, were chosen accordingly. The boundary conditions are:

- for $0 \leq x \leq l$:

$$\widetilde{u}(x_*, y, z, t) = \begin{cases} \widetilde{u}_\infty \left[1 - (\frac{r}{d})^2\right], \text{ if } 0 \leq x_* \leq l, \text{ and } r \leq d; \\ 0.23\widetilde{u}_\infty, \text{ if } 0 \leq x_* \leq l, \text{ and } d \leq r \leq D; \\ 0.02\widetilde{u}_\infty, \text{ otherwise;} \end{cases} \tag{5.11}$$

$$\widetilde{v}(x, y, z, t) = 0; \tag{5.12}$$

$$\widetilde{w}(x, y, z, t) = 0; \tag{5.13}$$

$$\widetilde{Z}(x_*, y, z, t) = \begin{cases} 1, \text{ if } 0 \leq x_* \leq l, \text{ and } r \leq d; \\ 0, \text{ otherwise;} \end{cases} \tag{5.14}$$

$$\widetilde{Y_F}(x_*, y, z, t) = \begin{cases} Y_{F,u}, \text{ if } 0 \leq x_* \leq l, \text{ and } r \leq d; \\ 0, \text{ otherwise;} \end{cases} \tag{5.15}$$

$$\widetilde{Y_{O_2}}(x_*, y, z, t) = \begin{cases} 0, \text{ if } 0 \le x_* \le l, \text{ and } r \le d; \\ Y_{O_2,u}, \text{ otherwise;} \end{cases} \tag{5.16}$$

$$\widetilde{Y_P}(x, y, z, t) = 0; \tag{5.17}$$

$$\widetilde{T}(x, y, z, t) = T_\infty; \tag{5.18}$$

$$\frac{\partial \overline{p}}{\partial x}(x, y, z, t) = 1; \tag{5.19}$$

$$\overline{\rho}(x, y, z, t) = \rho_\infty. \tag{5.20}$$

- for $x = L$:

$$\frac{\partial \widetilde{u}}{\partial x}(L, y, z, t) = \frac{\partial \widetilde{v}}{\partial x}(L, y, z, t) = \frac{\partial \widetilde{w}}{\partial x}(L, y, z, t) = 0; \tag{5.21}$$

$$\frac{\partial \widetilde{Z}}{\partial x}(L, y, z, t) = \frac{\partial \widetilde{T}}{\partial x}(L, y, z, t) = \frac{\partial \overline{\rho}}{\partial x}(L, y, z, t) = 0; \tag{5.22}$$

$$\frac{\partial \widetilde{Y_F}}{\partial x}(L, y, z, t) = \frac{\partial \widetilde{Y_{O_2}}}{\partial x}(L, y, z, t) = \frac{\partial \widetilde{Y_P}}{\partial x}(L, y, z, t) = 0; \tag{5.23}$$

$$\overline{p}(L, y, z, t) = 1. \tag{5.24}$$

- for $y = 0$:

$$\frac{\partial \widetilde{u}}{\partial y}(x, 0, z, t) = \frac{\partial \widetilde{v}}{\partial y}(x, 0, z, t) = \frac{\partial \widetilde{w}}{\partial y}(x, 0, z, t) = 0; \tag{5.25}$$

$$\frac{\partial \widetilde{Z}}{\partial y}(x, 0, z, t) = \frac{\partial \widetilde{T}}{\partial y}(x, 0, z, t) = \frac{\partial \overline{\rho}}{\partial y}(x, 0, z, t) = 0; \tag{5.26}$$

$$\frac{\partial \widetilde{Y_F}}{\partial y}(x, 0, z, t) = \frac{\partial \widetilde{Y_{O_2}}}{\partial y}(x, 0, z, t) = \frac{\partial \widetilde{Y_P}}{\partial y}(x, 0, z, t) = 0; \tag{5.27}$$

$$\frac{\partial \overline{p}}{\partial y}(x, 0, z, t) = 0. \tag{5.28}$$

- for $y = h$:

$$\frac{\partial \widetilde{u}}{\partial y}(x, h, z, t) = \frac{\partial \widetilde{v}}{\partial y}(x, h, z, t) = \frac{\partial \widetilde{w}}{\partial y}(x, h, z, t) = 0; \tag{5.29}$$

$$\frac{\partial \widetilde{Z}}{\partial y}(x, h, z, t) = \frac{\partial \widetilde{T}}{\partial y}(x, h, z, t) = \frac{\partial \overline{\rho}}{\partial y}(x, h, z, t) = 0; \tag{5.30}$$

$$\frac{\partial \widetilde{Y_F}}{\partial y}(x, h, z, t) = \frac{\partial \widetilde{Y_{O_2}}}{\partial y}(x, h, z, t) = \frac{\partial \widetilde{Y_P}}{\partial y}(x, h, z, t) = 0; \tag{5.31}$$

$$\frac{\partial \overline{p}}{\partial y}(x, h, z, t) = 0. \tag{5.32}$$

- for $z = 0$:

$$\frac{\partial \widetilde{u}}{\partial z}(x,y,0,t) = \frac{\partial \widetilde{v}}{\partial z}(x,y,0,t) = \frac{\partial \widetilde{w}}{\partial z}(x,y,0,t) = 0; \tag{5.33}$$

$$\frac{\partial \widetilde{Z}}{\partial z}(x,y,0,t) = \frac{\partial \widetilde{T}}{\partial z}(x,y,0,t) = \frac{\partial \overline{\rho}}{\partial z}(x,y,0,t) = 0; \tag{5.34}$$

$$\frac{\partial \widetilde{Y_F}}{\partial z}(x,y,0,t) = \frac{\partial \widetilde{Y_{O_2}}}{\partial z}(x,y,0,t) = \frac{\partial \widetilde{Y_P}}{\partial z}(x,y,0,t) = 0; \tag{5.35}$$

$$\frac{\partial \overline{p}}{\partial z}(x,y,0,t) = 0. \tag{5.36}$$

- for $z = h$:

$$\frac{\partial \widetilde{u}}{\partial z}(x,y,h,t) = \frac{\partial \widetilde{v}}{\partial z}(x,y,h,t) = \frac{\partial \widetilde{w}}{\partial z}(x,y,h,t) = 0; \tag{5.37}$$

$$\frac{\partial \widetilde{Z}}{\partial z}(x,y,h,t) = \frac{\partial \widetilde{T}}{\partial z}(x,y,h,t) = \frac{\partial \overline{\rho}}{\partial z}(x,y,h,t) = 0; \tag{5.38}$$

$$\frac{\partial \widetilde{Y_F}}{\partial z}(x,y,h,t) = \frac{\partial \widetilde{Y_{O_2}}}{\partial z}(x,y,h,t) = \frac{\partial \widetilde{Y_P}}{\partial z}(x,y,h,t) = 0; \tag{5.39}$$

$$\frac{\partial \overline{p}}{\partial z}(x,y,h,t) = 0. \tag{5.40}$$

6 NUMERICAL SOLVERS

To numerically solve the reactive turbulent flow equations, we discretize the equations using the finite difference method and integrate them using the Rosenbrock method.

6.1 Finite Difference Method

First, to numerically solve a problem in CFD, the spatial and time domain must be discretized, that is, they are divided into a finite number of steps. In a three-dimensional geometry, we divide each of the total lengths into the three x, y and z directions considering certain $\Delta x, \Delta y$ and Δz increments, respectively. In this context, the domain will be divided into cells of volumes $\Delta x \Delta y \Delta z$ bounded by nodes (x, y, z).

The finite difference method approximates the derivatives of the differential equation by the differences of the values of the function [99] at each domain node and at each time step. The derivative is replaced by the incremental ratio that converges to the derivative when the increment approaches zero. If the differential equation depends on more variables, the same process is applied separately for each of the variables.

Let x_0 belong to the domain and h a positive number. Mesh nodes can be defined by setting $x_i = x_0 \pm ih$, for $i = 1, 2, \ldots, n$; where h represents the length of the cell in the direction containing x_0. The approximations of a function $f(x)$ and its derivatives are calculated at the nodes of the mesh. For a three-dimensional problem, this procedure is done in all three directions.

A classic method for computing derivative approximations is the Taylor series [35], which relates values of the function and derivatives at a point x using

values in a neighborhood of x named $f(x+h)$. If $f(x)$ has derivatives up to the order $n+1$ in x, we have:

$$f(x+h) = f(x) + hf'(x) + \frac{h}{2!}f''(x) + \cdots + \frac{h}{n!}f^{(n)}(x) + \frac{h}{n+1!}f^{(n+1)}(\xi) \qquad (6.1)$$

with $x < \xi < x+h$.

We choose the type of finite difference to be applied to each term of the equations system from the analysis of the physical behavior of each term [35].

I) Spatial partial derivative of 1^{st} order – central finite differences of 2^{nd} order:

$$\left(\frac{\partial f}{\partial x}\right)_{(i,j,k)} \cong \frac{f^{(n)}_{(i+1,j,k)} - f^{(n)}_{(i-1,j,k)}}{2\Delta x}; \qquad (6.2)$$

$$\left(\frac{\partial f}{\partial y}\right)_{(i,j,k)} \cong \frac{f^{(n)}_{(i,j+1,k)} - f^{(n)}_{(i,j-1,k)}}{2\Delta y}; \qquad (6.3)$$

$$\left(\frac{\partial f}{\partial z}\right)_{(i,j,k)} \cong \frac{f^{(n)}_{(i,j,k+1)} - f^{(n)}_{(i,j,k-1)}}{2\Delta z}. \qquad (6.4)$$

II) Spatial partial derivative of 2^{nd} order – central finite differences of 2^{nd} order:

$$\left(\frac{\partial^2 f}{\partial x^2}\right)_{(i,j,k)} \cong \frac{f^{(n)}_{(i+1,j,k)} - 2f^{(n)}_{(i,j,k)} + f^{(n)}_{(i-1,j,k)}}{(\Delta x)^2}; \qquad (6.5)$$

$$\left(\frac{\partial^2 f}{\partial y^2}\right)_{(i,j,k)} \cong \frac{f^{(n)}_{(i,j+1,k)} - 2f^{(n)}_{(i,j,k)} + f^{(n)}_{(i,j-1,k)}}{(\Delta y)^2}; \qquad (6.6)$$

$$\left(\frac{\partial^2 f}{\partial z^2}\right)_{(i,j,k)} \cong \frac{f^{(n)}_{(i,j,k+1)} - 2f^{(n)}_{(i,j,k)} + f^{(n)}_{(i,j,k-1)}}{(\Delta z)^2}; \qquad (6.7)$$

where $\Delta x = x_{i+1} - x_i$, $\Delta y = y_{j+1} - y_j$ and $\Delta z = z_{k+1} - z_k$.

6.2 Rosenbrock Method

Rosenbrock method is suitable for stiff problems [88], and it requires the solution of a system of linear equations at each iteration step. This procedure is

simpler to solve and it has also a lower computational cost. Considering the system of differential equations with initial values:

$$\begin{cases} \dfrac{\partial V}{\partial t} & = \widetilde{\Phi}(V), \\ V(t_0) & = V_0; \end{cases} \tag{6.8}$$

the Rosenbrock method is now defined by:

$$V_{n+1} = V_n + \Delta t \sum_{i=1}^{s} \psi_i \Gamma_i, \tag{6.9}$$

where V is the vector of variables, $s = 4$ is the method order, Δt is the time step, ψ_i are method weights, and Γ_i are the method coefficients. These coefficients are calculated by:

$$\Gamma_i = \widetilde{\Phi}\left(V_n + \Delta t \sum_{j=1}^{i-1} a_{ij}\Gamma_j\right) + \phi\ \Delta t\ \frac{\partial \widetilde{\Phi}}{\partial V}\left(V_n + \sum_{j=1}^{i-1} b_{ij}\Gamma_j\right)\Gamma_i; \tag{6.10}$$

where a_{ij}, b_{ij} and ϕ are method parameters. For the fourth-order method, it is well accepted to take the values described in the table (6.2) as these values are in the stability region.

We can also use the variable time step Δt to reduce the computational cost. The choice of the size of Δt is made from an error analysis Ξ for certain tolerances $\epsilon \geq 0$. First, we estimate the local truncation error in each iteration as:

$$\Xi_{n+1} = \frac{||y^*_{n+1} - y_{n+1}||}{(2^s - 1)}, \tag{6.11}$$

where the term y^* is calculated using Δt while y is calculated using $\Delta t/2$.

The weighted norm $||.||$ is defined by [20]:

$$||y|| = \sqrt{\frac{1}{m}\sum_{i=1}^{m}\left(\frac{y^i_{n+1}}{y^i_{max}}\right)^2}. \tag{6.12}$$

Therefore, we define the size of the step Δt according to the following conditions [26]:

Table 6.1: Parameters for the fourth-order Rosenbrock method.

Parameters	Values
ψ_1	0,9451564786
ψ_2	0,3413231720
ψ_3	0,5655139575
ψ_4	-0,8519936081
a_{21}	-0,5
a_{31}	-0,1012236115
a_{32}	0,9762236115
a_{41}	-0,3922096763
a_{42}	0,7151140251
a_{43}	0,1430371625
b_{ij}	$0, \ \forall \ ij$
ϕ	0,57281606625

- If $\Xi_{n+1} > \epsilon$, the step is discarded and Δt is halved;
- If $3\epsilon/4 < \Xi_{n+1} < \epsilon$, the step is accepted, but Δt is halved;
- If $\epsilon/10 < \Xi_{n+1} < 3\epsilon/4$, both step and Δt are accepted;
- If $\Xi_{n+1} < \epsilon/10$, the step is accepted and Δt is duplicated.

7 NUMERICAL RESULTS

In this chapter, we present the numerical results obtained for the turbulent jet diffusion flame and for pollutant formation and oxidation resulting from the biofuel combustion. The biofuels used were methanol, to validate the numerical procedure adopted, and the MD, a biodiesel surrogate.

We use the Laboratório Integrado de Computação Científica at Instituto de Matemática e Estatística (LICC/IME - UFRGS), whose hardware configurations are: Intel(R) Core(TM) i7-4820K processor, 3.70 GHz CPU and 32GB of RAM memory. The computational code was developed and implemented in fortran 90 language, using double precision. The figures of the numerical experiments were generated in Scilab 6.0.1 or Gnuplot 5.2.4 software for Linux operating system.

Figure (7.1) shows the mixture fraction field, in which the largest mixture gradients occur at the pre-inlet pipes of the fuel jet, and decreases as the fuel moves away from the inlet and it mixes with the oxidant by convection and diffusion. The mixing in the jet depends on its speed. Higher velocities imply in larger mixture regions [40]. In the potential core region, the parabolic character of the fuel jet is observed.

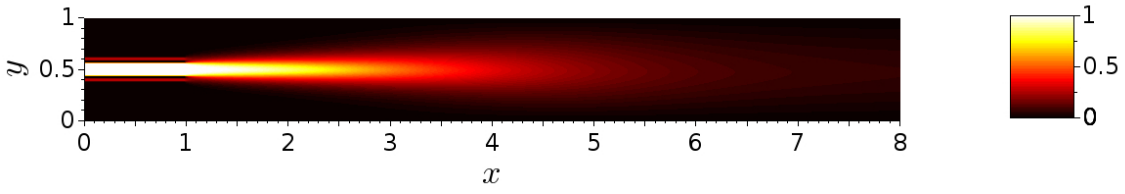

Figure 7.1: Mixture fraction field of MD flame in the range [0,8].

The mixture fraction profile, in the centerline of the jet, is compared with experimental data of the mixture fraction profile of the Sandia Flame D [8]. Figure (7.2) shows the comparison between the two profiles, which show good agree-

ment. The domain of the mixture profile was normalized by the diameter of the pre-inlet pipes of the fuel jet, to facilitate the comparison with results from the literature, as well as the indication of correspondence between the quantities.

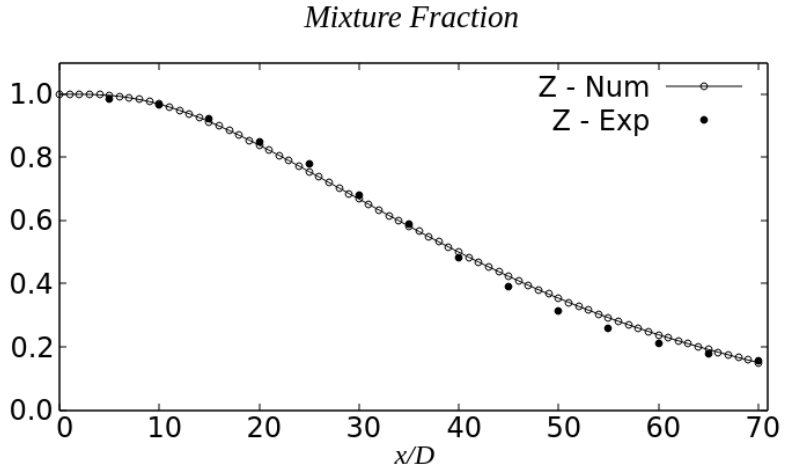

Figure 7.2: Comparison of the numerically obtained mixture fraction with experimental data [8] in the centerline of the MD flame.

As experimental data on the production of pollutants in the MD combustion are scarce in the literature, the numerical procedure was validated for the results in two steps. In the first step, we analyze a methanol flame and compare its results with the literature and, later, we apply the same procedure for a MD flame.

We compare the results obtained for the oxidant (O_2), water vapor (H_2O), temperature and pollutants: CO, CO_2 and NO_x , with the work of Muller et al. (1993) [64] and Glaude et al. (2014) [39]. In both works, experimental data are provided for a methanol flame.

Figures 7.3.(a) and 7.3.(b) show the mass fractions of the oxidant O_2 and the water vapor H_2O , respectively. The initial value of the oxidant mass fraction in the given free current was $Y_{O_2,2} = 0.23$, decreasing as the oxidant was consumed. For methanol, the initial value taken was $Y_{CH_3OH,1} = 1$.

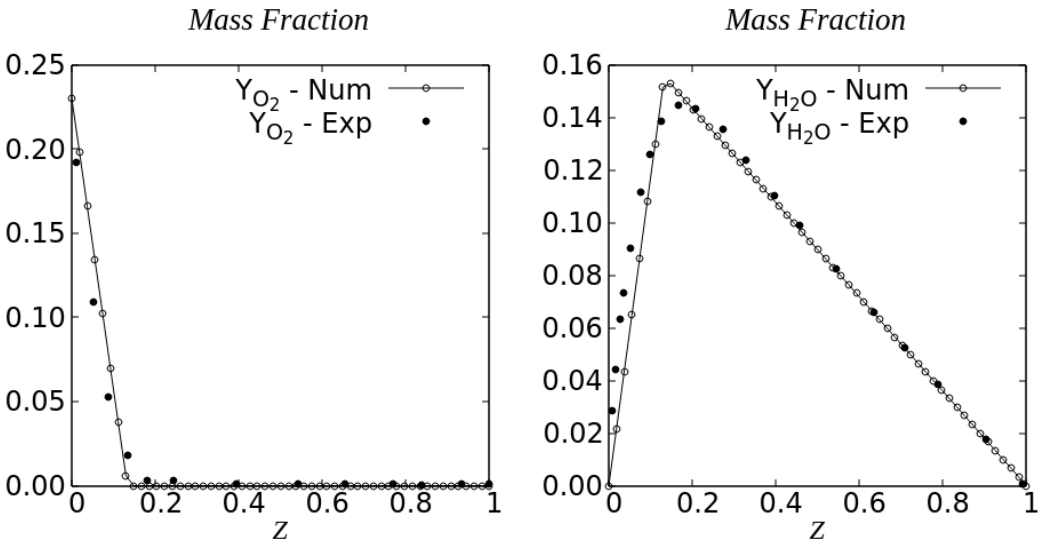

(a) (b)

Figure 7.3: Comparison with experimental data [64] for: (a) O_2 mass fraction and (b) H_2O mass fraction, as a function of the mixture fraction (Z), in a methanol flame.

The values $Z = 0$ and $Z = 1$ are the extremes of the mixture fraction space and represent cases where the mixture is composed purely of oxidizer $(Z = 0)$ or fuel $(Z = 1)$. At these points, therefore, the mass fractions of the other combustion products are null. As the values of the mixing fraction Z vary in the set of points $(0, 1)$, the mass fractions of H_2O, CO and CO_2 also vary, reaching their maximum values close to the stoichiometric region of the flame, $Z_{st} \simeq 0.16$, where conditions are considered suitable for burning.

Figure 7.4.(a) shows the curve of the mass fraction of CO, which was not presented in the work by Muller et al. (1993) [64], and the comparison between the mass fractions of CO_2 in the mixing fraction space. Although there is no information in the work by Muller et al. (1993) [64] on the mass fraction of CO, it can be assumed that the data obtained are acceptable, and that the generation of CO is significant for temperatures greater than $1500K$, so that for $Z \lesssim 0.1$, the mass fraction of CO is small.

Figure 7.4.(b) shows the temperature of the flame in the space of the mixture fraction. The initial ambient temperature is $298K$ and the adiabatic methanol flame temperature is approximately $2200K$. The adiabatic flame temperature is reached when there is no energy loss by the system. The energy conservation equation for temperature is complex and its source term contains parameters that are difficult to determine, thus, it is customary to calculate the temperature by the Burke-Schumann solution [67, 74, 76, 103], whose approximations are reasonable.

The Burke-Schumann equation for temperature is a piecewise function, which depends on the stoichiometric mixture fraction (Z_{st}). The maximum temperature values occur in the vicinity of the stoichiometric mixture fraction and tend to decrease as the mixture fraction values move away from Z_{st}.

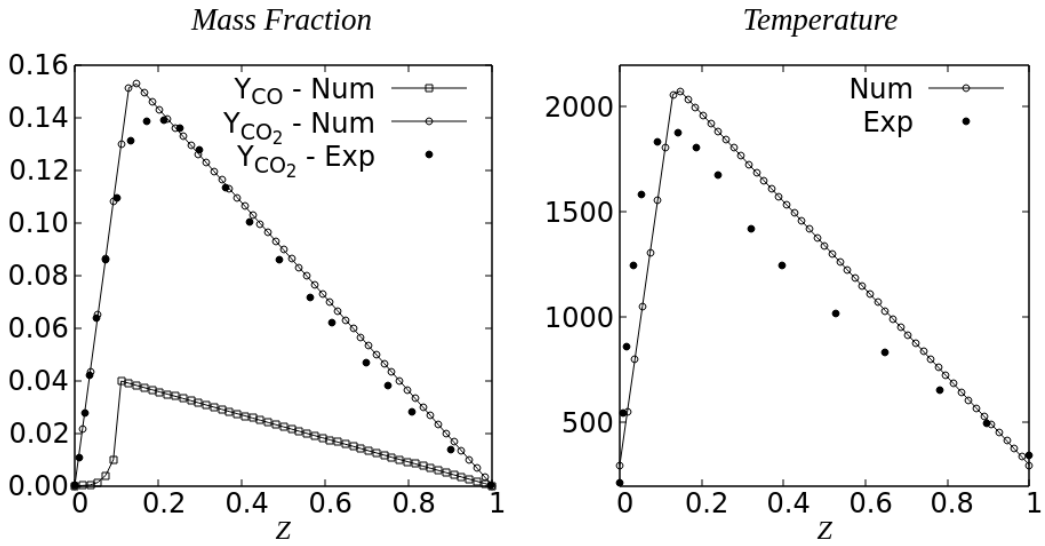

(a) (b)

Figure 7.4: Comparison with experimental data [64] for: (a) CO_2 mass fraction and (b) temperature (K), as a function of the mixture fraction (Z), in a methanol flame.

Figure 7.5.(a) shows the comparison between the molar fractions of NO, obtained numerically in this work with the experimental data of Glaude et. al

(2014) [39], regarding the fraction of the mixture (Z). In Fig. 7.5.(b), we add the curve for the molar fraction NO calculated from the Zel'dovich mechanism and the N_2O-intermediate mechanism, adding the formation rate given in Eq. (3.15) for the source term. The NO mass fraction appears as a peak, reaching high values close to the stoichiometric region of the flame.

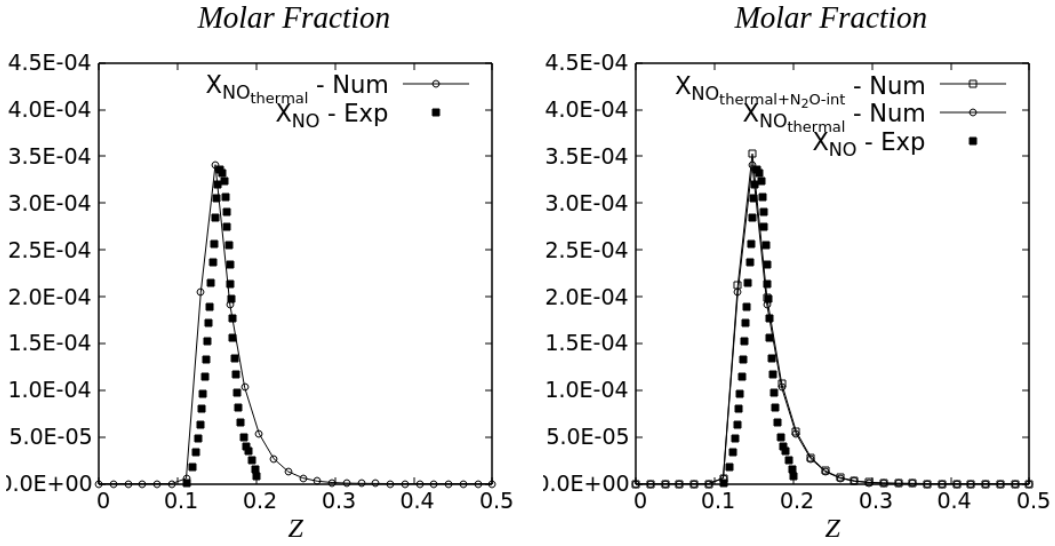

Figure 7.5: Comparison of numerical results with experimental data [39] for: (a) NO molar fraction obtained by the Zel'dovich mechanism; (b) NO molar fraction obtained using Zel'dovich and N_2O-intermediate mechanisms, along the mixture fraction (Z) in a methanol flame.

As the obtained results compare well with the literature data, for the methanol flame, the equations considering the MD flame were implemented and the results will be shown in the next section.

7.1 Results for NO_x

To equate the results obtained for the MD flame and for the methanol flame, we consider an initial condition for the free fuel stream of $Y_{MD,1} = 0.55$, that is, the fuel-air ratio for MD flame requires a lower percentage of fuel than methanol to achieve the same burning conditions.

Figures 7.6.(a) and 7.6.(b) illustrate the mass fractions of O_2, CO and CO_2, respectively, compared with the experimental data from Muller et al. (1993) [64]. The behavior of mass fractions agrees with those in the literature. In this case, it was found that, while the maximum value of CO increased in relation to the value obtained for the methanol flame, there was a significant reduction in the maximum value of CO_2, as shown in the table (7.1).

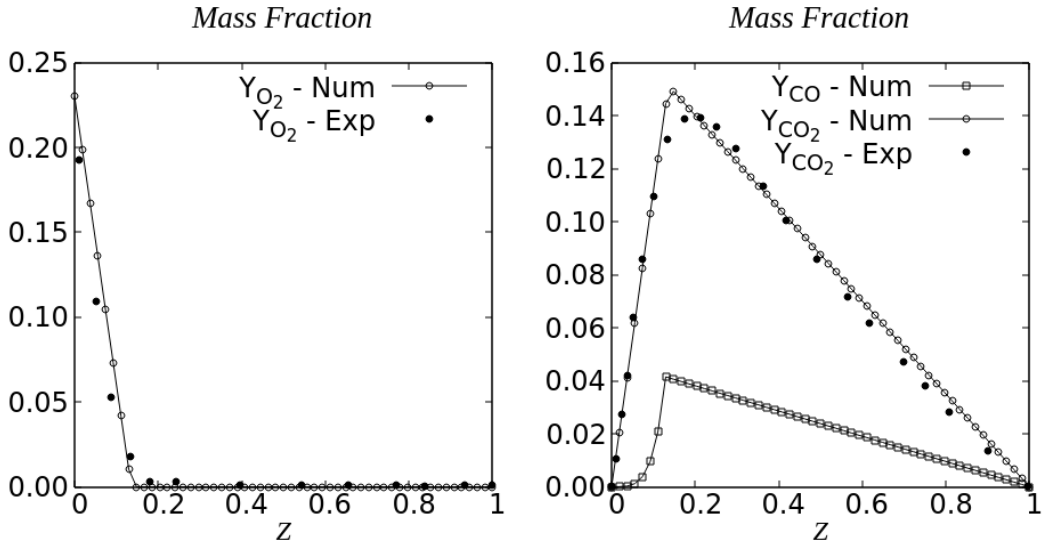

(a) (b)

Figure 7.6: Comparison with experimental data [64] for: (a) O_2 mass fraction and (b) CO and CO_2 mass fraction, as a function of the mixture fraction (Z), in a MD flame.

Table 7.1: Maximum values of CO and CO_2 mass fractions.

	Methanol	MD
CO	3.977×10^{-2}	4.145×10^{-2}
CO_2	0.153	0.149

Figure (7.7) shows the MD flame temperature in the mixture fraction space, calculated from the Burke-Schumann solution. The numerical results obtained for the flame temperature MD follow according to the data provided by Muller et al. (1993) [64].

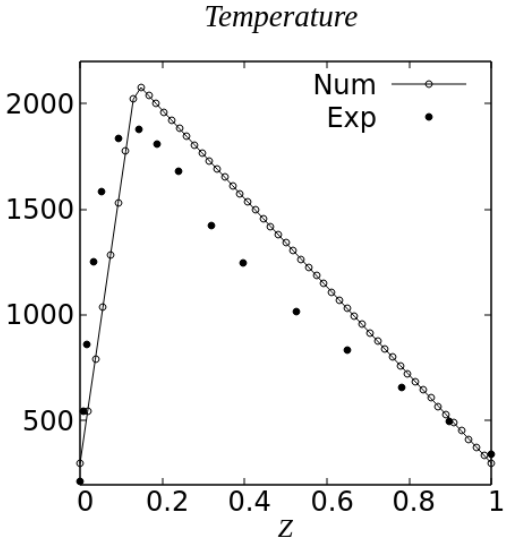

Figure 7.7: Comparison with experimental data [64] for the temperature, as a function of the mixture fraction (Z), in the MD flame.

Figures 7.8.(a) and 7.8.(b) show comparisons between the NO mass fractions obtained in this work and in the work by Glaude et. al (2014) [39]. In the Fig. (a), the NO formation rate corresponds only to the Zel'dovich mechanism, while in the Fig. (b) the Zel'dovich and N_2O - intermediary mechanisms were considered. There is good agreement between the results. The maximum NO values for the MD

flame are closer to the maximum values obtained by Glaude et al. (2014) than for a methanol flame, as shown in the table (7.2).

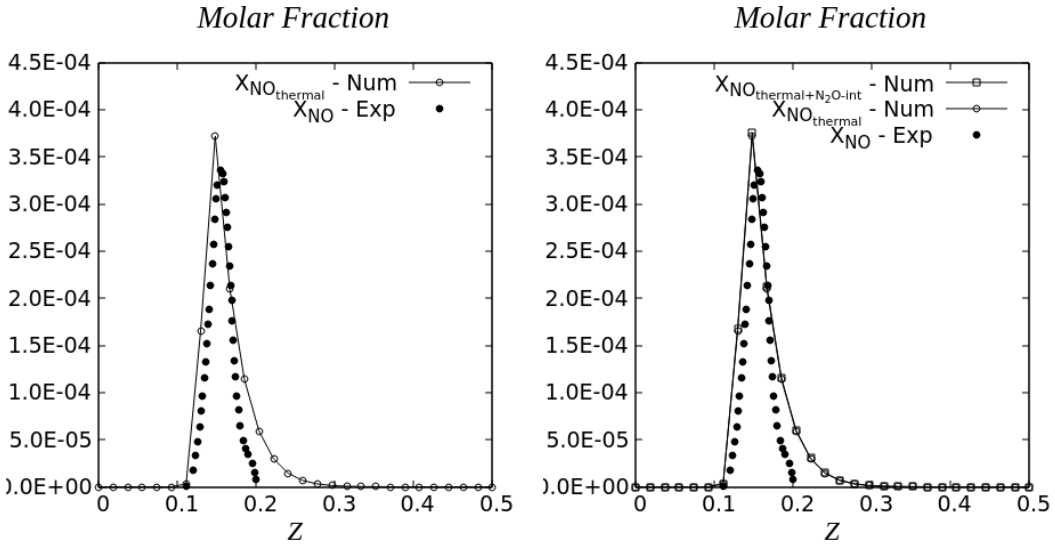

(a) (b)

Figure 7.8: Comparison of numerical results with experimental data [39] for: (a) NO molar fraction obtained by the Zel'dovich mechanism; (b) NO molar fraction obtained using the Zel'dovich and N_2O-intermediate mechanisms, along the mixture fraction (Z) in a MD flame.

Table 7.2: Maximum values of the NO mass fractions.

Exp. [39]	Num. - CH_3OH	Num. - MD	
3.357×10^{-4}	3.410×10^{-4}	3.372×10^{-4}	Thermal
	3.527×10^{-4}	3.435×10^{-4}	Thermal + N_2O-int.

This case, we take the initial condition for the free stream fuel to be approximately $Y_{MD,1} = 0.063$ to adapt the stoichiometric region of the flame with [84]. We compare the mass fractions of the main species of the mechanism, such as CH_4, CO_2, H_2O, C_2H_2, C_2H_4, OH; and also the temperature.

Figures 7.9.(a) and 7.9.(b) illustrate the CO_2 and H_2O mass fractions, respectively. While the maximum values of CO_2 did not vary significantly from the previous situation for this case, we can verify that the maximum values of $H2O$ decreased approximately 34% compared to the methanol flame shown in Fig. 7.3.(b).

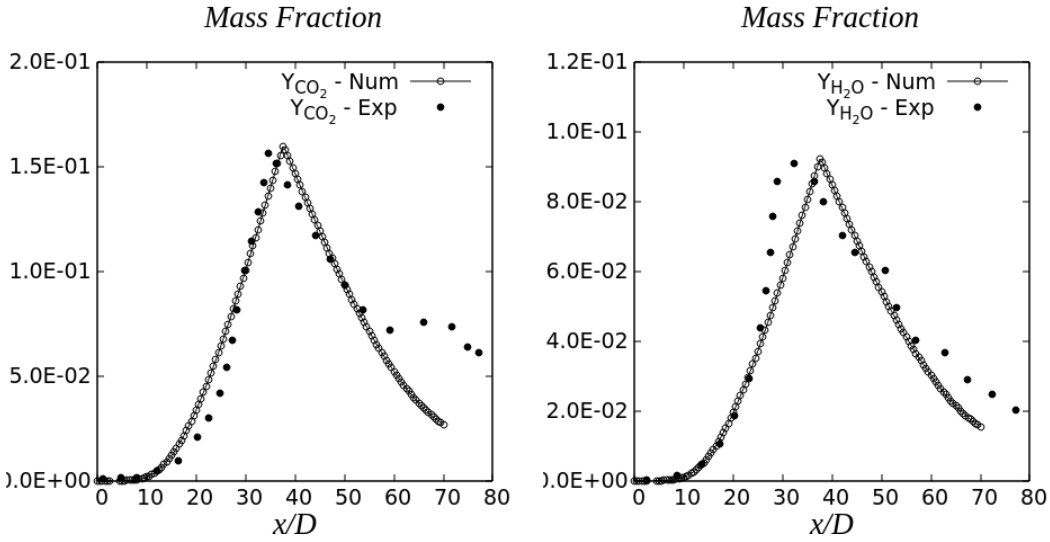

(a) (b)

Figure 7.9: Comparison with experimental data [84] for: (a) CO_2 mass fraction and (b) H_2O mass fraction in a MD flame.

We verified better agreement between the numerical results obtained and the data provided by [84] near the stoichiometric region of the flame, where the temperature gradients are higher. Far from this region, buoyancy observed in [84] was not captured in our model due to simplifications made in the study of turbulence.

Figures 7.10.(a) and 7.10.(b) illustrate the mass fractions of CH_4 and OH, respectively, while Figs. 7.11.(a) and 7.11.(b) show the mass fractions of C_2H_2

and C_2H_4. Although the last three species are not considered primary pollutants, they are important for the production of other pollutants, such as soot.

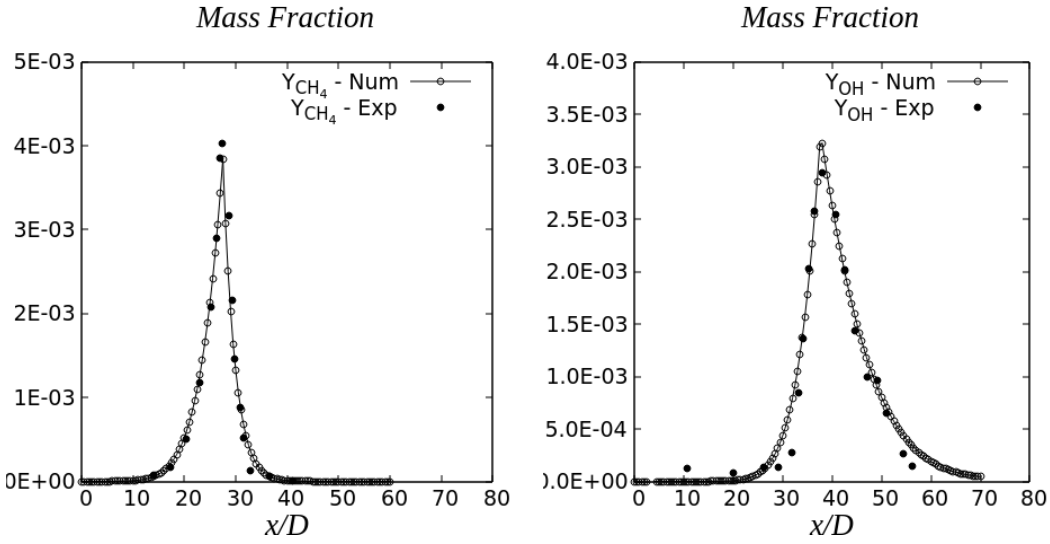

Figure 7.10: Comparison with experimental data [84] for: (a) CH_4 mass fraction and (b) OH mass fraction in a MD flame.

Figure 7.12 shows the temperature field, in Kelvin, and Fig. 7.13 illustrates the temperature at the centerline of the MD flame calculated by the Burke-Schumann solution. As an approximation of the function of temperature, the Burke-Schumann solution also did not capture the fluctuations seen far from the stoichiometric region of the flame. However, the peak temperature is reached in the same region, assuming maximum values close to 2200K.

Considering a 10% variation for the values obtained for the temperature, via the Burke-Schumann solution, Fig. 7.14 shows the comparative error with the data from Ref. [84]. We can see a significant similarity in the jet inlet region and also in the peak of the stoichiometric region of the flame.

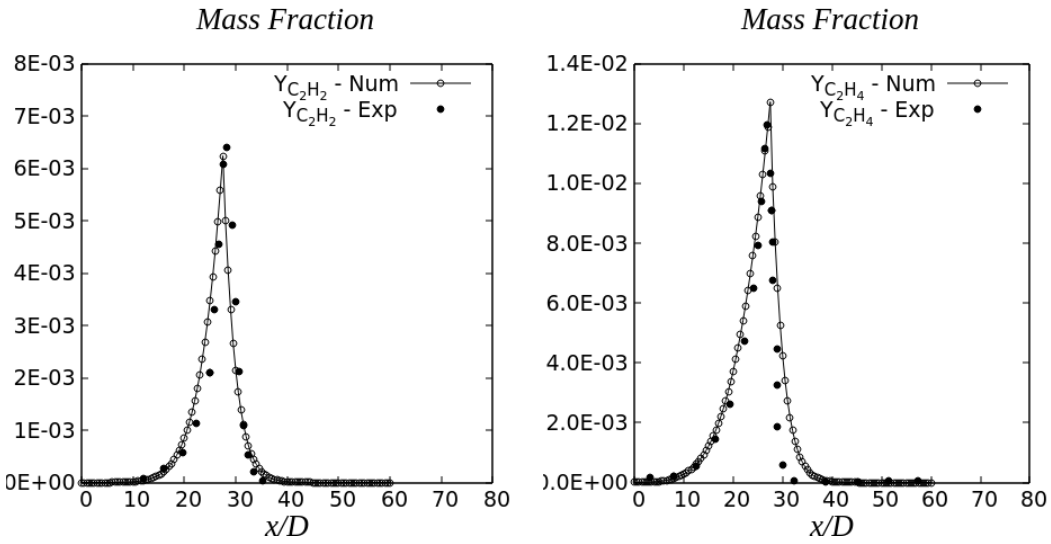

Figure 7.11: Comparison with experimental data [84] for: (a) C_2H_2 mass fraction and (b) C_2H_4 mass fraction in a MD flame.

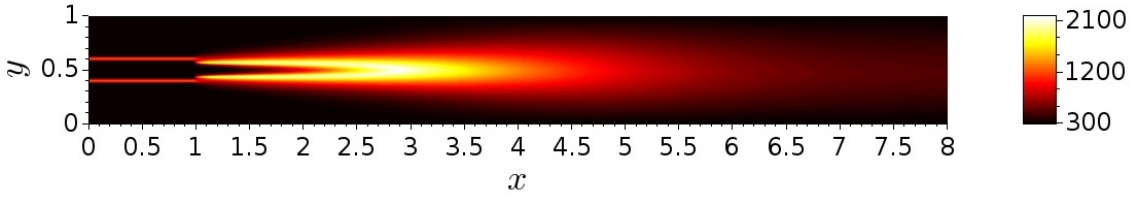

Figure 7.12: Temperature (K) field of MD flame.

Considering the results presented, and their agreement with the literature, we calculated the NO molar fraction using the Zel'dovich mechanism and N_2O-intermediate mechanism, as shown in Figs. 7.15.(a) and 7.15.(b).

We observed that the peak behavior of the NO mass fraction in the stoichiometric region of the flame is maintained, as well as its order of magnitude. The increase of 1×10^{-4} in the NO mass fraction, in relation to the case analyzed previously in Fig. (7.8), may be associated with the fact that the mechanism contains

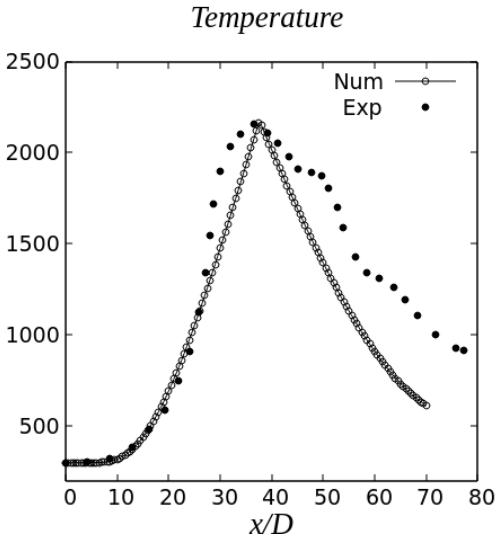

Figure 7.13: Comparison with experimental data [84] for temperature (K) in a MD flame.

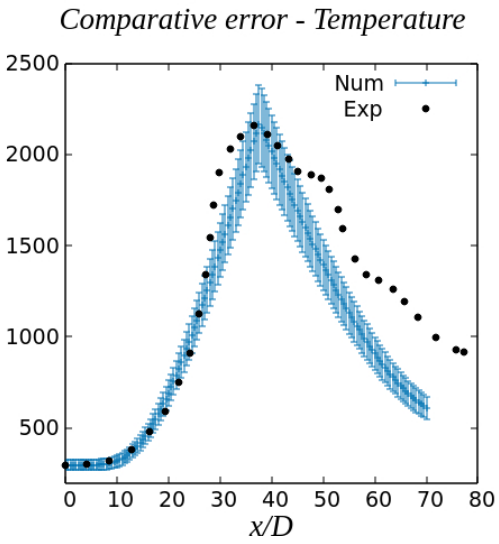

Figure 7.14: Comparative temperature (K) error [84] in a MD flame.

a larger number of species that influence the production of NO, as well as by the variation of the initial free flow fuel-nitrogen ratio.

Figure 7.16 illustrates the NO mass fraction field, using Zel'dovich and N_2O-intermediate mechanisms, in order to visualize its bidimensional behavior. In

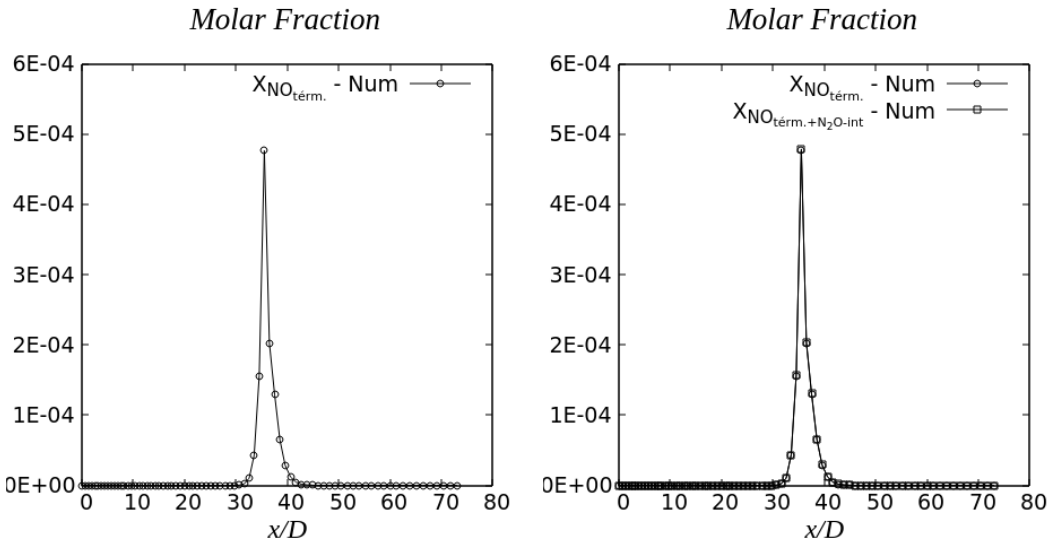

Figure 7.15: Molar fraction of NO obtained by: (a) Zel'dovich mechanism; (b) Zel'dovich and N_2O-intermediate mechanisms, in a MD flame.

fact, the maximum values of the NO mass fraction are obtained in the jet centerline near to the region of higher flame temperature gradients.

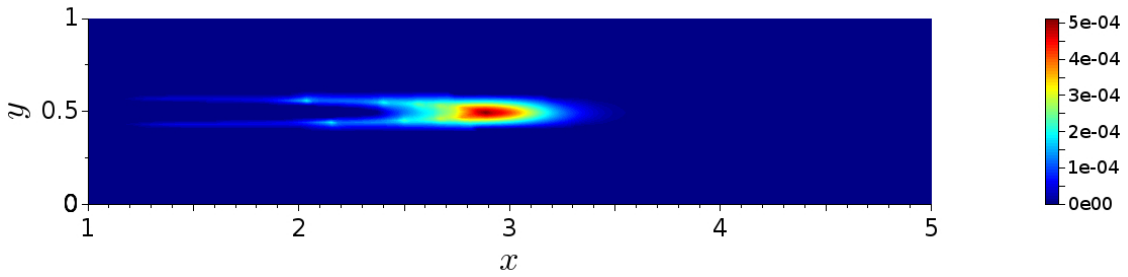

Figure 7.16: NO mass fraction field.

7.2 Results for Soot

In the study of the soot emission prediction, we consider the turbulent jet diffusion flame of MD, under the same conditions as above, and we change the flame stoichiometric region, when possible and necessary, to relate it to works already published in the scientific community.

First, we consider the 5-step mechanism for fuel oxidation and the mechanism of Kronenburg et al. (2000) [47] for the soot production. In the work presented by Kronenburg et al. (2000) [47], the soot emission prediction model was tested for a methane flame; nonetheless, it is plausible to use it in other hydrocarbon fuels (and oxygenated hydrocarbons) larger than the methane molecule, since methane is part of the main combustion chain of these fuels.

We take $Y_{MD,1} = 1.0$ and then consequently, $Z_{st} \simeq 0.08$, as close as possible to the stoichiometric region shown in Ref. [47] for the methane flame. Figures 7.17.(a) and 7.17.(b) illustrate the mass fractions of the species C_2H_2 and OH in the mixture fraction space.

About C_2H_2, the maximum values reached are close although smaller in MD flame. As for the OH, we see greater discrepancies, although they are on the same magnitude scale, the volume fraction of OH for MD flame is considerably smaller. In Ref. [47], the largest gradients of OH occur slightly to the left of the stoichiometric region, which we could not predict in our model.

We solve the mass fraction (Y_{C_S}) and soot particle number of particles (N_S) equations and compare them with the data from Ref. [47]. Figures 7.18.(a) and 7.18.(b) show the comparisons. We verified a reduction in the mass fraction and soot particle number density in the MD flame. The reduction in soot emission can be related to the chosen fuel, model simplifications, as well as the reduction of the soot precursors mass fractions.

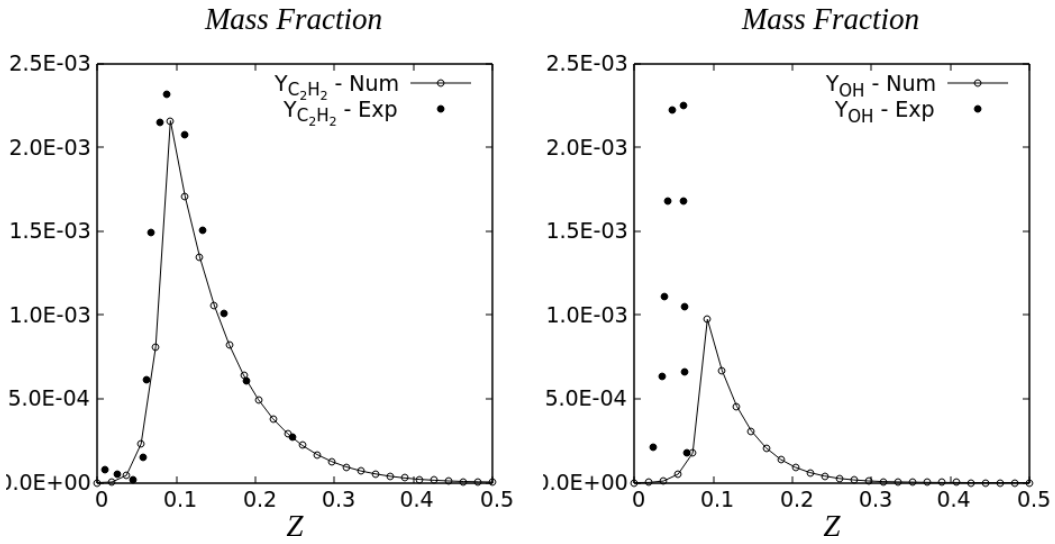

(a) (b)

Figure 7.17: Comparison with experimental data [47] for: (a) C_2H_2 mass fraction and (b) OH mass fraction in a MD flame.

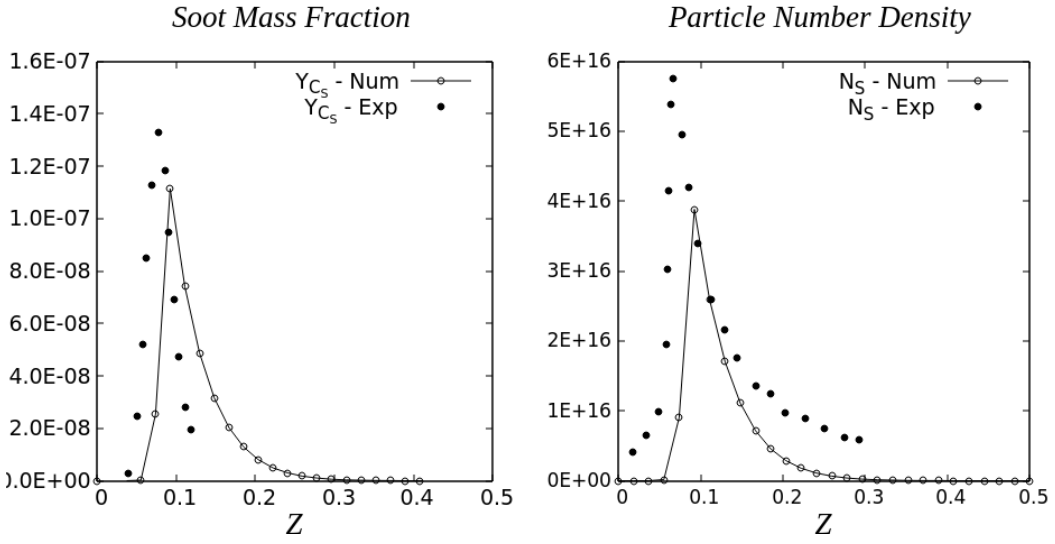

(a) (b)

Figure 7.18: Comparison with experimental data [47] for: (a) Y_{C_S} mass fraction and (b) N_S particle number density in a MD flame.

Cai et al. (2016) [21] applied the semi-empirical model for soot formation in a surrogate biodiesel flame composed by MD, $MD9D$ and n-heptane. The authors used the ABF mechanism [4] to describe the formation reactions of the $PAHS$ soot precursors. In this work, in order to simplify the model, we consider a reduced mechanism based in ABF mechanism, containing the main elementary reactions [38] of the formation of C_2H_2, C_2H_3 and OH.

We take $Y_{MD,1} \simeq 0.3$, obtaining $Z_{st} \simeq 0.22$, stoichiometric region of the flame in Ref. [21]. Figures 7.19.(a) and 7.19.(b) show the mass fractions of the precursor species of soot, which are in agreement with the authors' data. The use of the HACA mechanism for the soot formation adjusts the maximum values for the species C_2H_2, C_2H_3 and OH. This is a factor that influences the difference between the results obtained in this case, for C_2H_2 and OH, and the case exposed in Figs. 7.10.(b) and 7.11.(a).

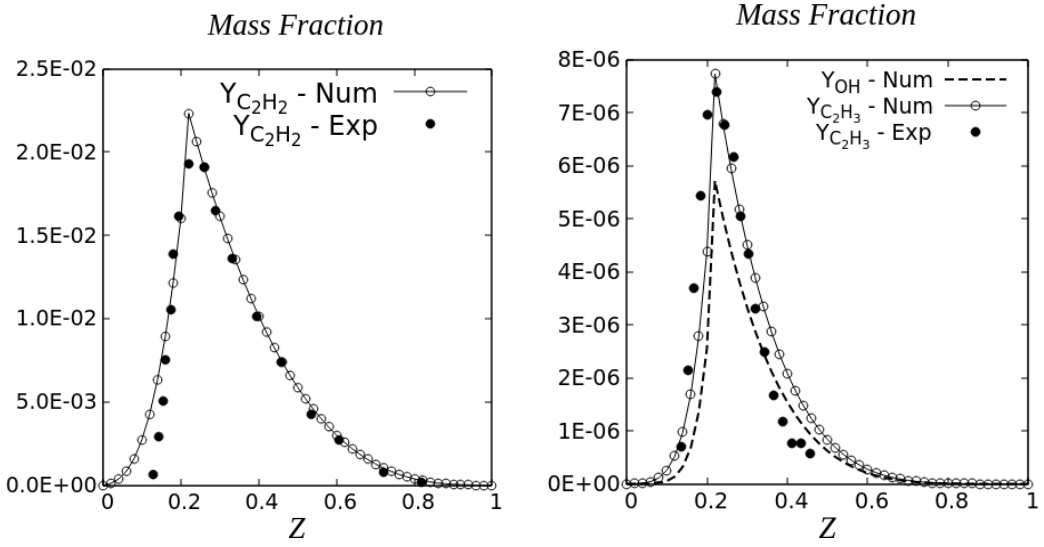

(a) (b)

Figure 7.19: Comparison with experimental data [21] for: (a) C_2H_2 mass fraction and (b) C_2H_3 mass fraction in a MD flame.

Figure 7.20 illustrates the comparison of soot volume fractions. The authors show that the soot prediction is 78% lower in surrogate biodiesel flame when compared to petroleum diesel flame, calculated from the semi-empirical model. Nevertheless, it should be noted that the maximum values of the soot volume fraction are an order of magnitude higher than the values generally found in the literature [6, 95, 101].

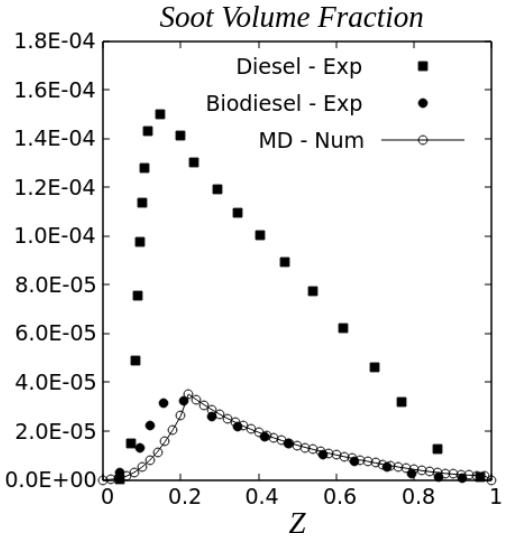

Figure 7.20: Comparison with experimental data [21] for soot volume fraction in a MD flame.

Finally, we combine the reduced 26-step mechanism for MD oxidation, the Zel'dovich and N_2O-intermediate mechanism for the formation of NO_x and the simplified mechanism for the formation of soot, in order to analyze the pollutants prediction at the same time.

We take $Y_{MD,1} = 0.063$, as done earlier in the comparative case with Ref. [84] and exposed in Fig. 7.15. We solve the soot mass fraction equation, and Fig. 7.21 illustrates the obtained curve.

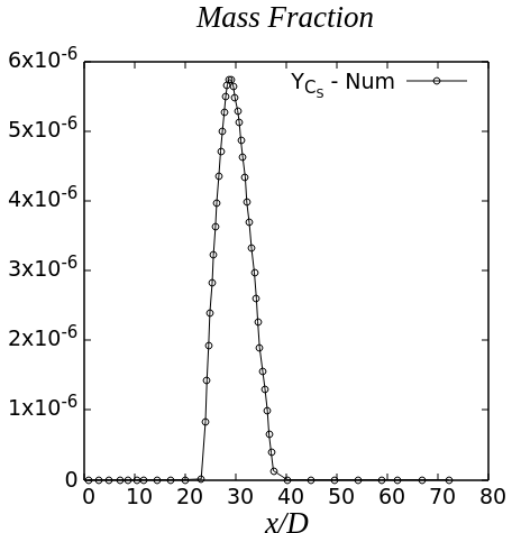

Figure 7.21: Soot mass fraction in a MD flame.

Figure 7.22 shows the bidimensional field of the soot mass fraction, in which we notice a spatial behavior similar to that of NO_x, where the largest gradients of pollutants occur near the stoichiometric region of the flame.

In perspective, the NO_x maximum values are two orders of magnitude greater than the soot maximum values. By the other hand, the soot distribution area is larger than that of NO_x.

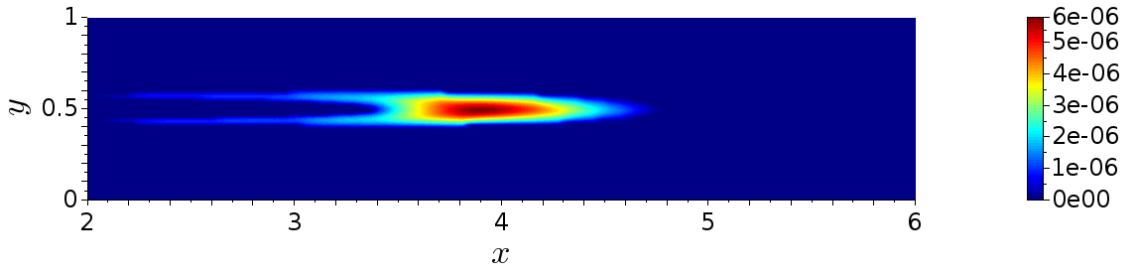

Figure 7.22: Soot mass fraction field.

8 FINAL CONCLUSIONS

Environmentally and economically viable alternatives are increasingly being sought in order to reduce dependence on the use of fossil fuels, which come from non-renewable energy sources and which will become scarce and more expensive in a few years.

Methods that numerically quantify with precision the emission of pollutants, such as NO_x and soot, generated in the combustion of different biodiesel/surrogates compositions, contribute to social and environmental aspects, and may suggest improvements in combustion processes, reducing costs and emissions pollutants; and technological and research aspects, as they describe a reduced kinetic mechanism for the modeling of a biodiesel surrogate.

There are numerous phenomena associated with the emission of pollutants during turbulent mixture, reaction and biodiesel combustion, which are still not understood. The main contribution of this research is the mathematical modeling and simulation of pollutants in the combustion of the most representative biodiesel surrogate: methyl decanoate.

We investigated the generation of two atmospheric pollutants, NO_x and soot, emitted during the combustion of MD through simulations of a turbulent diffusion flame. We consider the Navier-Stokes equations for reactive flow, the conservation equation for mass fractions of chemical species, and the Burke-Schumann solution to approximate concentrations of certain species. We analyzed the behavior of the flame jet, its velocity, the mixture fraction, the temperature and the emission of NO_x and soot for certain flame conditions.

We consider different reduced kinetic mechanisms, both for MD combustion and for the formation and oxidation of NO_x and soot pollutants, since one

of our goals is to obtain results in agreement with the literature while the computational cost of the modeling is feasible.

In this work, we adopt an approach that has several techniques coupled to make the modeling of the problem as complete as possible. We did a study on the appropriate kinetic mechanisms for the formation of pollutants. For MD combustion, we first work with global mechanisms and then we improve the modeling considering a reduced kinetic mechanism using the DRG technique.

Turbulence was treated using the LES technique and eddy viscosity was approximated by both the Agrawal-Prasad and Smagorinsky models. We did a dimensional analysis of the problem in order to expose the important combinations of parameters. And then, we numerically solve the system of equations using the Rosenbrok Method. Finally, we compared the results obtained with data released by other researchers.

Differently from other works already published, we use pure MD as a biofuel instead of biofuel mixtures. Results in this direction are still scarce and we aim to progressively contribute in this direction, whether including other pollutants, testing other kinetic mechanisms and improving the study and modeling of biofuel surrogates.

BIBLIOGRAPHY

[1] Agrawal, A., and Prasad, A. K. Integral solution for the mean flow profiles of turbulent jets, plumes, and wakes. *Journal of Fluids Engineering 125*, 5 (2003), 813.

[2] Alfonsi, G. Reynolds-averaged Navier-Stokes equations for turbulence modeling. *Applied Mechanics Reviews 62* (2009), 040802.

[3] Angelovič, M., Tkáč, Z., and Angelovič, M. Particulate emissions and biodiesel: A review. *Scientific Papers: Animal Science and Biotechnologies 46* (2013), 192–198.

[4] Appel, J., Bockhorn, H., and Frenklach, M. Kinetic modeling of soot formation with detailed chemistry and physics: laminar premixed flames of C_2 hydrocarbons. *Combustion and Flame 121*, 1 (2000), 122–136.

[5] Aris, R. *Vectors, Tensors, and the Basic Equations of Fluid Mechanics*. Dover Publications Inc., New York, 1989.

[6] Bai, Y., Wang, Y., and Wang, X. Development of a skeletal mechanism for four-component biodiesel surrogate fuel with PAH. *Renewable Energy 171* (2021), 266–274.

[7] Bajpai, P. Production of biofuel from microalgae. In *Third Generation Biofuels*. Springer, Singapore, 2019, pp. 45–66.

[8] Barlow, R., and Frank, J. Piloted CH_4/air flames C, D, E and F - release 2.0. 2019. <https://www.sandia.gov/TNF/DataArch/FlameD.html>.

[9] Barlow, R., Frank, J., Karpetis, A., and Chen, J.-Y. Piloted methane/air jet flames: Transport effects and aspects of scalar structure. *Combustion and Flame 143*, 4 (2005), 433–449.

[10] Bart, J. C. J., Palmeri, N., and Cavallaro, S. *Biodiesel science and technology: From soil to oil.* Woodhead Publishing Series in Energy: Number 7. Woodhead Publishing Limited, 2010.

[11] Basu, P. *Biomass Gasification, Pyrolysis, and Torrefaction: Practical Design and Theory*, 2 ed. Elsevier, 2013.

[12] Beschkov, V. *Biogas, Biodiesel and Bioethanol as Multifunctional Renewable Fuels and Raw Materials.* IntechOpen, 2017, pp. 187–205.

[13] Bisetti, F., Blanquart, G., and Pitsch, H. Direct numerical simulation of soot formation in turbulent non-premixed flames. *Center for Turbulence Research - Annual Research Briefs* (2008), 437–449.

[14] Bleecker, M. L. Carbon monoxide intoxication. In *Occupational Neurology*, vol. 131. Elsevier, 2015, pp. 191–203.

[15] Boussinesq, J. *Theorie de l'écoulement tourbillant et tumultueux des liquides.* Gauthier–Villars et fils, 1897.

[16] Bozzelli, J. W., and DEAN, A. M. O + NNH: A possible new route for NO_x formation in flames. *International Journal of Chemical Kinetics 27* (1995), 1097– 1109.

[17] Brunetti, F. *Mecânica dos Fluidos, 2. ed.* Pearson Prentice Hall, 2008.

[18] Brusseau, M. L., Matthias, A. D., Comrie, A. C., and Musil, S. A. Atmospheric pollution. In *Environmental and Pollution Science (Third Edition)*, M. L. Brusseau, I. L. Pepper, and C. P. Gerba, Eds., third edition ed. Academic Press, 2019, pp. 293–309.

[19] Buckley, N. A., Juurlink, D. N., Isbister, G., Bennett, M. H., and Lavonas, E. J. Hyperbaric oxygen for carbon monoxide poisoning. *Cochrane Database of Systematic Reviews 4* (2011), 339–354.

[20] Bui, T. D., and Bui, T. R. Numerical methods for extremely stiff systems of ordinary differential equations. *Applied Mathematical Modelling 3*, 5 (1979), 355–358.

[21] Cai, G., Yen, M., and Abraham, J. On formulating a simplified soot model for diesel and biodiesel combustion. *Chemical Engineering Science 144* (2016), 249–259.

[22] Chang, H. Prediction of soot formation in laminar opposed diffusion flame with detailed and reduced reaction mechanisms. Master's thesis, School of Aerospace Engineering, Georgia Institute of Technology, 2004.

[23] Chen, L., and Ghoniem, A. F. Modeling CO_2 chemical effects on CO formation in oxy-fuel diffusion flames using detailed, quasi-global, and global reaction mechanisms. *Combustion Science and Technology 186* (2014), 829–848.

[24] Cheng, Y., Lien, F. S., E., Y., and Sinclair, R. A comparison of large eddy simulations with a standard $k - \varepsilon$ Reynolds-averaged Navier–Stokes model for the prediction of a fully developed turbulent flow over a matrix of cubes. *Journal of Wind Engineering and Industrial Aerodynamics 91*, 11 (2003), 1301–1328.

[25] de Bortoli, A. L. *Introduction to Computational Fluid Dynamics*. Editora da UFRGS, 2000. In Portuguese.

[26] de Bortoli, A. L., Andreis, G. S. L., and Pereira, F. N. *Modeling and Simulation of Reactive Flows*. Elsevier Science Publishing, 2015.

[27] Demirbas, A. Importance of biodiesel as transportation fuel. *Energy Policy 35*, 9 (2007), 4661–4670.

[28] Demirbas, A. *Biofuels: Securing the Planet's Future Energy Needs*. Springer, 2009.

[29] Diévart, P., Won, S. H., Dooley, S., Dryer, F. L., and Ju, Y. A kinetic model for methyl decanoate combustion. *Combustion and Flame 159*, 5 (2012), 1793–1805.

[30] Dragone, G., Fernandes, B., Vicente, A., and Teixeira, J. *Third generation biofuels from microalgae*, vol. 2. Formatex Research Center, 2010, pp. 1355 – 1366.

[31] El-Zoheiry, R., Elseesy, A., Attia, A., He, Z., and El-Batsh, H. Combustion and emission characteristics of jojoba biodiesel-jet A1 mixtures applying a lean premixed pre-vaporized combustion techniques: An experimental investigation. *Renewable Energy* (10 2020).

[32] Faravelli, T., Ranzi, E., Frassoldati, A., Cuoci, A., and Mehl, M. The CRECK Modeling Group, Outubro 2021. "`http://creckmodeling.chem.polimi.it`".

[33] Fenimore, C. P. Formation of nitric oxide in premixed hydrocarbon flames. *Thirteenth Symposium (International) on Combustion 13* (1971), 373–380.

[34] Fernando, S., Hall, C., and Jha, S. NO_x reduction from biodiesel fuels. *Energy & Fuels 20*, 1 (2006), 376–382.

[35] Ferziger, J. H., and Peric, M. *Computacional methods for fluid dynamics*, 3 ed. Springer, 2002.

[36] Floyd, J., and Mcgrattan, K. Multiple parameter mixture fraction with two-step combustion chemistry for large eddy simulation. *International Interflam Conference 11th Proceedings* (2007).

[37] Frassoldati, A., Cuoci, A., Faravelli, T., Niemann, U., Ranzi, E., Seiser, R., and Seshadri, K. An experimental and kinetic modeling study of n-propanol and iso-propanol combustion. *Combustion and Flame 157*, 1 (2010), 2–16.

[38] Frenklach, M. Reaction mechanism of soot formation in flames. *Physical Chemistry Chemical Physics 4* (2002), 2028–2037.

[39] Glaude, P. A., Sirjean, B., Fournet, R., Bounaceur, R., Vierling, M., Montagne, P., and Molière, M. Combustion and oxidation kinetics of alternative gas turbines fuels. *Proceedings of ASME Turbo Expo 2014: Turbine Technical Conference and Exposition* (2014).

[40] Gokarn, A., Battaglia, F., Fox, R. O., and Hill, J. C. Simulations of mixing for a confined co-flowing planar jet. *Computers & Fluids 35* (2006), 1228–1238.

[41] Golovitchev, V. I., and Yang, J. Construction of combustion models for rapeseed methyl ester bio-diesel fuel for internal combustion engine applications. *Biotechnology Advances 27*, 5 (2009), 641–655.

[42] Habib, M. A., Elshafei, M., and Dajani, M. Influence of combustion parameters on NO_x production in an industrial boiler. *Computers & Fluids 37* (2008), 12–23.

[43] Herbinet, O., J. Pitz, W., and Westbrook, C. Detailed chemical kinetic mechanism for the oxidation of biodiesel fuels blend surrogate. *Combustion and Flame 157* (2009), 893–908.

[44] Hinze, J. O. *Turbulence: An Introduction to its Mechanism and Theory.* McGraw-Hill, 1959.

[45] Jiang, B., Liang, H., Huang, G., and Li, X. Study on NO_x formation in CH_4/air jet combustion. *Chinese Journal of Chemical Engineering 14*, 6 (2006), 723–728.

[46] Kralova, I., and Sjöblom, J. Biofuels - renewable energy sources: A review. *Journal of Dispersion Science and Tecnology 31* (2010), 409–425.

[47] Kronenburg, A., Bilger, R. W., and Kent, J. H. Modeling soot formation in turbulent methane–air jet diffusion flames. *Combustion and Flame 121*, 1 (2000), 24 – 40.

[48] Lele, A. D., Anand, K., and Narayanaswamy, K. *Surrogates for Biodiesel: Review and Challenges.* Springer, 2017.

[49] Leon, S. J. *Álgebra Linear com Aplicações.* LTC Editora, 1999.

[50] Leung, K. M., and Lindstedt, R. P. Detailed kinetic modeling of C1-C3 alkane diffusion flames. *Combustion and Flame 102* (1995), 129–160.

[51] Leung, K. M., Lindstedt, R. P., and Jones, W. P. A simplified reaction mechanism for soot formation in nonpremixed flames. *Combustion and Flame 87*, 3-4 (1991), 289–305.

[52] Li, S. C., Williams, F. A., and Gebert, K. A simplified, fundamentally based method for calculating NO_x emissions in lean premixed combustors. *Combustion and Flame 119*, 3 (1999), 367–373.

[53] Lu, T., and Law, C. K. A directed relation graph method for mechanism reduction. *Proceedings of the Combustion Institute 30* (2005), 333–1341.

[54] Lu, T., and Law, C. K. Linear time reduction of large kinetic mechanisms with directed relation graph: n-heptane and iso-octane. *Combustion and Flame 144*, 1 (2006), 24–36.

[55] Lu, T., and Law, C. K. On the applicability of directed relation graphs to the reduction of reaction mechanisms. *Combustion and Flame 146* (2006), 472–483.

[56] Luque, R., and Speight, J. G. *Gasification for Synthetic Fuel Production: Fundamentals, Processes, and Applications.* Woodhead Publishing Series in Energy: Number 69. Woodhead Publishing Limited, 2015.

[57] Maliska, C. R. *Heat Transfer and Computational Fluid Mechanics.* Livro Técnico e Científico, 1995. In Portuguese.

[58] Malte, P. C., and Pratt, D. T. Measurement of atomic oxygen and nitrogen oxides in jet-stirred combustion. *Fifteenth Symposium (International) on Combustion 15*, 1 (1975), 1061 – 1070.

[59] Masri, A. R., Dibble, R. W., and Barlow, R. S. The structure of turbulent nonpremixed flames revealed by Raman-Rayleigh-LIF measurements. *Progress in Energy and Combustion Science 22*, 4 (1996), 307–362.

[60] Mass, U., and Pope, S. B. Simplifying chemical kinetics: intrinsic low-dimensional manifolds in composition space. *Combustion and Flame 88* (1992), 239–264.

[61] Michelsen, H. A., Colket, M. B., Bengtsson, P.-E., D'Anna, A., Desgroux, P., Haynes, B. S., Miller, J. H., Nathan, G. J., Pitsch, H., and Wang, H. A review of terminology used to describe soot formation and evolution under combustion and pyrolytic conditions. *ACS Nano 14*, 10 (2020), 12470–12490.

[62] Ministério de Minas e Energia. *Brazilian Energy Review. Base Year 2020*, julho 2021. In Portuguese.

[63] Mollenhauer, K., and Tschöke, H. *Handbook of Diesel Engines.* Springer, 2010.

[64] Müller, C. M., Seshadri, K., and Chen, J. Y. *Reduced Kinetic Mechanisms for counterflow methanol diffusion flammes. In: Reduced Kinetic Mechanisms for Applications in Combustion Systems.* Lecture Notes in Physics Series. Springer-Verlag GmbH, 1993.

[65] Naik, C. V., Westbrook, C. K., Herbinet, O., Pitz, W. J., and Mehl, M. Detailed chemical kinetic reaction mechanism for biodiesel components

methyl stearate and methyl oleate. *Proceedings of the Combustion Institute 33* (2011), 383–389.

[66] Nakao, A., Sugimoto, R., Billiara, T. R., and McCurry, K. R. Therapeutic Antioxidant Medical Gas. *Journal of Clinical Biochemistry and Nutrition 44* (2009), 1–13.

[67] Nayagam, V., Dietrich, D. L., and Williams, F. A. A Burke-Schumann analysis of diffusion-flame structures supported by a burning droplet. *Combustion Theory and Modelling 21* (2017), 646–657.

[68] Ogunkunle, O., and Ahmed, N. A. Overview of biodiesel combustion in mitigating the adverse impacts of engine emissions on the sustainable human–environment scenario. *Sustainability 13*, 10 (2021).

[69] Omidvarborna, H., Kumar, A., and Kim, D.-S. NO_x emissions from low-temperature combustion of biodiesel made of various feedstocks and blends. *Fuel Processing Technology 140* (2015), 113 – 118.

[70] Owolabi, R. U., Adejumo, A. L., and Aderibigbe, A. F. Biodiesel: Fuel for the future (a brief review). *International Journal of Energy Engineering* (2012), 223–231.

[71] Palash, S., Kalam, M., Masjuki, H., Masum, B., Rizwanul Fattah, I., and Mofijur, M. Impacts of biodiesel combustion on no_x emissions and their reduction approaches. *Renewable and Sustainable Energy Reviews 23* (2013), 473–490.

[72] Pepiot-Desjardins, P., Pitsch, H., Malhotra, R., Kirby, S. R., and Boehman, A. L. Structural group analysis for soot reduction tendency of oxygenated fuels. *Combustion and Flame 154*, 1-2 (2008), 191–205.

[73] Peters, N. *Systematic reduction of flame kinetics: Principles and Details*. American Institute of Astronautics and Aeronautics, 1988, pp. 67–86.

[74] Peters, N. Fifteen lectures on laminar and turburlent combustion. < https://www.itv.rwth-aachen.de/fileadmin/Downloads/Summerschools/SummerSchool.pdf >, 1992.

[75] Peters, N., and Rogg, B. *Reduced Kinetic Mechanisms for Applications in Combustion Systems*. Lecture Notes in Physics Series. Springer-Verlag, 1993.

[76] Pitsch, H. Laminar Premixed Flames. *CEFRC Combustion Summer School. 10 July. 2019* (2014), Disponível em < https://cefrc.princeton.edu >.

[77] Pitsch, H., and Steiner, H. Large-eddy simulation of a turbulent piloted methane/air diffusion flame (Sandia Flame D). *Physics of Fluids 12*, 10 (2000), 2541–2554.

[78] Porumbel, I., and Menon, S. *Simulation of Soot Formation in Diffusion Jet Flame Using Linear Eddy Model*. 2003.

[79] Raine, R. R., Stone, C. R., and Gould, J. Modeling of nitric oxide formation in spark ignition engines with a multizone burned gas. *Combustion and Flame 102*, 3 (1995), 241–255.

[80] Rajasekar, E., Murugesan, A., Subramanian, R., and Nedunchezhian, N. Review of NO_x reduction technologies in CI engines fuelled with oxygenated biomass fuels. *Renewable and Sustainable Energy Reviews 14*, 7 (2010), 2113–2121.

[81] Ranzi, E., Cavallotti, C., Cuoci, A., Frassoldati, A., Pelucchi, M., and Faravelli, T. New reaction classes in the kinetic modeling of low temperature oxidation of n-alkanes. *Combustion and Flame 162*, 5 (2015), 1679–1691.

[82] Ranzi, E., Frassoldati, A., Grana, R., Cuoci, A., Faravelli, T., Kelley, A., and Law, C. Hierarchical and comparative kinetic modeling of

laminar flame speeds of hydrocarbon and oxygenated fuels. *Progress in Energy and Combustion Science 38*, 4 (2012), 468–501.

[83] RANZI, E., FRASSOLDATI, A., STAGNI, A., PELUCCHI, M., CUOCI, A., AND FARAVELLI, T. Reduced kinetic schemes of complex reaction systems: Fossil and biomass-derived transportation fuels. *International Journal of Chemical Kinetics 46*, 9 (2014), 512–542.

[84] RASSOULINEJAD-MOUSAVI, S. M., MAO, Y., AND ZHANG, Y. Reducing greenhouse gas emissions in Sandia methane-air flame by using a biofuel. *Renewable Energy 128* (2018), 313–323.

[85] REN21. *Renewables 2021 Global Status Report*, 2021.

[86] RENEWABLE FUELS ASSOCIATION (RFA). *Essencial Energy - 2021 Ethanol Industry Outlook*, August 2021.

[87] ROSENDAHL, L. *Biomass combustion science, technology and engineering.* Woodhead Publishing Series in Energy: Number 40. Woodhead Publishing Limited, 2013.

[88] SANDU, A., VERWER, J. G., BLOM, J. G., SPEE, E. J., CARMICHAEL, G. R., AND POTRA, F. A. Benchmarking stiff ODE solver for atmospheric chemistry problems II: Rosenbrock solvers. *Atmospheric Environment 31* (1997), 3459–3472.

[89] SARATHY, S. M., THOMSON, M. J., PITZ, W. J., AND LU, T. An experimental and kinetic modeling study of methyl decanoate combustion. *Proceedings of the Combustion Institute 33*, 1 (2011), 399–405.

[90] SARIN, R., KUMAR, R., SRIVASTAV, B., PURI, S. K., TULI, D. K., MALHOTRA, R. K., AND KUMAR, A. Biodiesel surrogates: Achieving performance demands. *Bioresource Technology 100*, 12 (2009), 3022 – 3028.

[91] Schraufnagel, D. E. The health effects of ultrafine particles. *Experimental & Molecular Medicine 52*, 3 (2020), 311–317.

[92] Shudo, T., Omori, K., and Hiyama, O. NO_x reduction and NO_2 emission characteristics in rich-lean combustion of hydrogen. *International Journal of Hydrogen Energy 33*, 17 (2008), 4689–4693.

[93] Sillman, S. Tropospheric ozone and photochemical smog. In *Treatise on Geochemistry*, H. D. Holland and K. K. Turekian, Eds., 2 ed. Elsevier, Oxford, 2014, pp. 415–437.

[94] Smagorinsky, J. General circulation experiments with the primitive equations. *Monthly Weather Review 91* (1963), 99–164.

[95] Smooke, M., Long, M., Connelly, B., Colket, M., and Hall, R. Soot formation in laminar diffusion flames. *Combustion and Flame 143*, 4 (2005), 613–628.

[96] Song, H. *Investigation on Nitric Oxide and Soot of Biodiesel and Conventional Diesel using a Medium Duty Diesel Engine.* PhD thesis, Texas A&M University, 2012.

[97] Souza, P. R. *Aeroacoustic Characterization of Subsonic Jets in Crossflow.* PhD thesis, Universidade Federal de Uberlândia, 2015.

[98] Spellman, F. A., and Bieber, R. M. *Environment Health and Science: Desk Reference.* Government Institutes, 2012.

[99] Strikwerda, J. C. *Finite difference schemes and partial differential equations.* Society for Industrial and Applied Mathematics, 1974.

[100] Ströher, G. L., Nicoleti, J. F., Andrade, C. R., Zaparoli, E. L., and Ströher, G. R. Analysis of the single point approach RANS for axisymmetric and incompressible free jet type flow. *Engevista 14*, 3 (2012). In Portuguese.

[101] Tian, B., Chong, C., Fan, L., Ng, J.-H., Zhang, C., and Hochgreb, S. Soot volume fraction measurements over laminar pool flames of biofuels, diesel and blends. *Proceedings of the Combustion Institute 37*, 1 (2019), 877–884.

[102] Tsuji, H. Counterflow diffusion flames. *Progress in Energy and Combustion Science 8*, 2 (1982), 93–119.

[103] Turns, S. R. *An Introduction To Combustion: Concepts and Applications*. McGrraw-Hill Inc., 2000.

[104] Vaz, F. A. *Modeling and Simulation of Turbulent Diffusion Flames of Ethanol*. PhD thesis, Universidade Federal do Rio Grande do Sul, 2013. In Portuguese.

[105] Waldron, K. *Bioalcohol production: Biochemical conversion of lignocellulosic biomass*. Woodhead Publishing Series in Energy: Number 3. Woodhead Publishing Limited, 2010.

[106] Wang, F., Liu, J., and Zeng, H. Interactions of particulate matter and pulmonary surfactant: Implications for human health. *Advances in Colloid and Interface Science 284*, 102244 (2020).

[107] Wang, Y., and Chung, S. H. Soot formation in laminar counterflow flames. *Progress in Energy and Combustion Science 74* (2019), 152 – 238.

[108] Warnatz, J., Maas, U., and Dibble, R. W. *Combustion*, 4 ed. Springer, 2006.

[109] Wellinger, A., Murphy, J., and Baxter, D. *The biogas handbook: Science, production and applications*. Woodhead Publishing Series in Energy: Number 52. Woodhead Publishing Limited, 2013.

[110] Westbrook, C. K., Naik, C. V., Herbinet, O., Pitz, W. J., Mehl, M., Sarathy, S. M., and Curran, H. J. Detailed chemical kinetic reaction

mechanisms for soy and rapeseed biodiesel fuels. *Combustion and Flame 158*, 4 (2011), 742–755.

[111] Westenberg, A. A. Kinetics of NO and CO in lean, premixed hydrocarbon–air flames. *Combustion Science and Technology 4* (1971), 59–64.

[112] Williams, F. A. Progress in knowledge of flamelet structure and extinction. *Progress in Energy and Combustion Science 26* (2000), 657–682.

[113] Zarli, A. Oleochemicals: all time players of green chemistry. In *Catalysis, Green Chemistry and Sustainable Energy*, A. Basile, G. Centi, M. D. Falco, and G. Iaquaniello, Eds., vol. 179 of *Studies in Surface Science and Catalysis*. Elsevier, 2020, pp. 77–95.

[114] Zel'dovich, Y., Frank-Kamenetskii, D. A., and Sadovnikov, P. Oxidation of nitrogen in combustion. *Publishing House of the Academy of Sciences of the USSR* (1947).

[115] Zhang, R., Tie, X., and Bond, D. W. Impacts of anthropogenic and natural NO_x sources over the U.S. on tropospheric chemistry. *Proceedings of the National Academy of Sciences 100*, 4 (2003), 1505–1509.

[116] Zhao, F., Yang, W., and Yu, W. A progress review of practical soot modelling development in diesel engine combustion. *Journal of Traffic and Transportation Engineering (English Edition) 7*, 3 (2020), 269–281.

[117] Zhou, L. Modeling of single-phase turbulence. In *Theory and Modeling of Dispersed Multiphase Turbulent Reacting Flows*, L. Zhou, Ed. Butterworth-Heinemann, 2018, pp. 89–120.